# Distinctive roles of air–sea coupling on different MJO events: A new perspective revealed from the DYNAMO/CINDY field campaign

**ARTICLE** *in* MONTHLY WEATHER REVIEW · MARCH 2015

Impact Factor: 3.36 · DOI: 10.1175/MWR-D-14-00221.1



**8 AUTHORS**, INCLUDING:

Xiouhua Fu
University of Hawai'i System
**44** PUBLICATIONS **2,077** CITATIONS
SEE PROFILE

June-Yi Lee
Pusan National University
**80** PUBLICATIONS **1,628** CITATIONS
SEE PROFILE

SPECIAL
DYNAMO/CINDY/AMIE/LASP
COLLECTION

# Distinctive Roles of Air–Sea Coupling on Different MJO Events: A New Perspective Revealed from the DYNAMO/CINDY Field Campaign*

XIOUHUA FU,[+] WANQIU WANG,[#] JUNE-YI LEE,[@] BIN WANG,[&] KAZUYOSHI KIKUCHI,[&] JINGWEI XU,[**] JUAN LI,[&] AND SCOTT WEAVER[#]

[+] *International Pacific Research Center, School of Ocean and Earth Science and Technology, University of Hawai'i at Mānoa, Honolulu, Hawaii, and Earth System Modelling Center, Nanjing University of Information Science and Technology, Nanjing, China*

[#] *Climate Prediction Center, NOAA/NWS/NCEP, College Park, Maryland*

[@] *International Pacific Research Center, School of Ocean and Earth Science and Technology, University of Hawai'i at Mānoa, Honolulu, Hawaii, and Pusan National University, Pusan, South Korea*

[&] *International Pacific Research Center, School of Ocean and Earth Science and Technology, University of Hawai'i at Mānoa, Honolulu, Hawaii*

[**] *Earth System Modelling Center, Nanjing University of Information Science and Technology, Nanjing, China*

(Manuscript received 11 June 2014, in final form 6 October 2014)

ABSTRACT

Previous observational analysis and modeling studies indicate that air–sea coupling plays an essential role in improving MJO simulations and extending MJO forecasting skills. However, whether the SST feedback plays an indispensable role for the existence of the MJO remains controversial, and the precise physical processes through which the SST feedback may lead to better MJO simulations and forecasts remain elusive.

The DYNAMO/Cooperative Indian Ocean Experiment on Intraseasonal Variability in the Year 2011 (CINDY) field campaign recently completed over the Indian Ocean reveals a new perspective and provides better data to improve understanding of the MJO. It is found that among the five MJO events that occurred during the DYNAMO/CINDY field campaign, only two MJO events (the November and March ones) have robust SST anomalies associated with them. For the other three MJO events (the October, December, and January ones), no coherent SST anomalies are observed. This observational scenario suggests that the roles of air–sea coupling on the MJO vary greatly from event to event.

To elucidate the varying roles of air–sea coupling on different MJO events, a suite of hindcast experiments was conducted with a particular focus on the October and November MJO events. The numerical results confirm that the October MJO is largely controlled by atmospheric internal dynamics, while the November MJO is strongly coupled with underlying ocean. For the November MJO event, the positive SST anomalies significantly improve MJO forecasting by enhancing the response of a Kelvin–Rossby wave couplet, which prolongs the feedback between convection and large-scale circulations, and thus favors the development of stratiform rainfall, in turn, facilitating the production of eddy available potential energy and significantly amplifying the intensity of the model November MJO.

## 1. Introduction

The Madden–Julian oscillation (MJO) is a dominant mode of tropical convection variability on intraseasonal time scales (Madden and Julian 1971; Zhang 2005; Lau and Waliser 2011). The MJO convective envelope usually initiates over equatorial Africa and the western equatorial Indian Ocean (Wang and Rui 1990a). The associated circulation systems propagate eastward as a Kelvin–Rossby wave couplet (Wang 1988a; Wang and Rui

* School of Ocean and Earth Science and Technology Contribution Number 9234, International Pacific Research Center Contribution Number 1092, and Earth System Modelling Center Contribution Number 23.

*Corresponding author address:* Dr. Joshua Xiouhua Fu, International Pacific Research Center, School of Ocean and Earth Science and Technology, University of Hawai'i at Mānoa, 1680 East West Rd., POST Bldg. 409D, Honolulu, HI 96822.
E-mail: xfu@hawaii.edu

DOI: 10.1175/MWR-D-14-00221.1

1990b; Hendon and Salby 1994; Roundy 2012). Through upscale/downscale impacts and tropical–extratropical teleconnections, the MJO modulates the weather and climate activities over the globe (Donald et al. 2006; Zhang 2013). The recurrent nature of the MJO with a period of 30–60 days also offers an opportunity to bridge the forecasting gap between medium-range weather forecast (~1 week) and seasonal prediction (~1 month and longer) (e.g., Waliser 2005; Fu et al. 2008a; Brunet et al. 2010; Hoskins 2013). However, most global research models and operational weather/climate models still face various challenges to realistically simulate and accurately predict the MJO (Lin et al. 2006; Vitart et al. 2007; Wang and Seo 2009; Rashid et al. 2011; Fu et al. 2011; Weaver et al. 2011; Matsueda and Endo 2011; Hung et al. 2013), therefore, severely hindering the prediction of MJO's global impacts (Vitart and Molteni 2010).

Before the launch of the TOGA COARE field campaign over the western equatorial Pacific (Webster and Lukas 1992), almost all theoretical and modeling studies treated the MJO as an atmospheric internal phenomenon; for example, the wave-CISK (conditional instability of the second kind) (e.g., Lau and Peng 1987; Chang and Lim 1988; Lau et al. 1988) and frictional convergence-CISK theories (Wang 1988a). The wind-induced surface heat exchange (WISHE) hypothesis raised by Emanuel (1987) and Neelin et al. (1987) aimed to advocate the essential role of oceanic surface evaporation on maintaining the MJO cycle. The assumption of mean easterly winds over Indo-western Pacific sector in their original framework, however, is at odds with the observations (Wang 1988b; Jones and Weare 1996) although follow-up studies suggest that nonlinear WISHE might play a certain role on MJO dynamics (e.g., Araligidad and Maloney 2008; Sobel et al. 2010).

Utilizing daily SST and surface wind datasets collected during the First Global Atmospheric Research Program (GARP) Global Experiment (FGGE) campaign (in 1979), Krishnamurti et al. (1988) documented the first observational evidence of atmosphere–ocean interactions on intraseasonal time scales: significant fluctuations of sea surface temperature (SST) and surface heat fluxes on 30–50 days present over the Indo-western Pacific warm-pool oceans. This pioneering work raises the potential importance of air–sea coupling on MJO dynamics, which motivated Krishnamurti to propose that "a combination of atmospheric internal instabilities and external SST forcing on intra-seasonal time scales may enhance the atmospheric responses toward an eventual satisfactory simulation of intra-seasonal oscillation."

Two MJO events along with coherent upper-ocean variability were first documented by the TOGA COARE field campaign from November 1992 to February 1993 (Yanai et al. 2000; Richards et al. 1995; Weller and Anderson 1996), although this program was geared to advance the understanding and prediction of El Niño–Southern Oscillation (ENSO; Webster and Lukas 1992). Using TOGA COARE in situ measurements, Anderson et al. (1996) and Stephens et al. (2004) showed that, during the MJO suppressed phase, the associated clear sky and weak surface winds enhance downward solar radiation, reduce surface evaporation, and shoal the upper-ocean mixed layer depth, thus resulting in a steady warm up of the western Pacific. In addition to the gradual warming on intraseasonal time scales, the sea surface temperature also rapidly fluctuates with amplitude of 1°–2°C on the diurnal time scale. The gradual warming on the intraseasonal time scale along with the rapid daytime warming of the sea surface destabilizes the atmospheric boundary layer and promotes the developments of shallow and congestus clouds (Johnson et al. 1999; Kikuchi and Takayabu 2004). The lower-tropospheric moistening and boundary layer convergence induced by these clouds (Wu 2003) precondition the outbreaks of organized deep convection, leading to the MJO active phase (Fu et al. 2006; Tao et al. 2009). The associated widespread clouds and westerly wind bursts, on the other hand, significantly reduce downward solar radiation and intensify surface evaporation (Shinoda et al. 1998) and upper-ocean entrainment (Fu et al. 2003; Han et al. 2007). All these processes work to cool the underlying sea surface and inhibit the SST diurnal cycle, eventually leading to the suppressed phase of the MJO again (Anderson et al. 1996). The above observational evidence shows that sea surface temperature and the upper ocean systematically responds to MJO atmospheric forcing, and simultaneously may also feed back to the atmosphere to regulate MJO evolutions (Stephens et al. 2004).

Using a hierarchy of models, most previous studies have shown that air–sea coupling significantly improves various aspects of the major observed MJO features; for example, its organization, strength, and propagation, as well as the quadrature precipitation–SST phase relationship (e.g., Krishnamurti et al. 1992; Flatau et al. 1997; Wang and Xie 1998; Waliser et al. 1999; Woolnough et al. 2000; Fu and Wang 2004; Maloney and Sobel 2004; Fu et al. 2007, 2008b; Pegion and Kirtman 2008; Marshall et al. 2008), with few suggesting otherwise (e.g., Hendon 2000; Chou and Hsueh 2010). Does the SST feedback play an indispensable role for the existence of the MJO? It is difficult to draw a definite answer from the existing observational, theoretical, and modeling studies. In fact, the MJO may largely owe its origin to atmospheric internal dynamics: primarily the coupling between organized convection and equatorial waves (Lau and Peng 1987; Chang and Lim 1988; Wang 1988a; Wang and Rui

1990b; Wang and Li 1994; Kikuchi and Wang 2010; Roundy 2012). A global cloud-system-resolving model also shows that the atmosphere-alone approach is able to largely reproduce an MJO event (Miura et al. 2007; Liu et al. 2009). Although substantial observational and modeling evidence points out the importance of interactive air–sea coupling on MJO dynamics, our knowledge of the degree of impacts of ocean coupling (Watterson 2002; Zhang et al. 2006; Hsu and Li 2012), and on the feedback processes from the ocean to the atmosphere (Waliser et al. 1999; Wang and Xie 1998; Johnson et al. 1999; Fu et al. 2006; Marshall et al. 2008; Fu et al. 2008b) and our capability of representing these processes in the state-of-the-art coupled general circulation models (GCMs) are still very limited (Lin et al. 2006; Wu et al. 2008; Hung et al. 2013).

One grand challenge faced by the weather and climate communities is to advance seamless forecasts (Palmer et al. 2008; Shukla et al. 2009), in which the primary forecast gap is on the intraseasonal time scale (Brunet et al. 2010). Recently, several internationally collaborative programs have been launched to address this issue; for example, the Year of Tropical Convection (YOTC) virtual field campaign (Moncrieff et al. 2012) and the DYNAMO/Cooperative Indian Ocean Experiment on Intraseasonal Variability in the Year 2011 (CINDY) in situ field campaign (Yoneyama et al. 2013). These programs not only obtain unprecedented high-quality atmospheric and oceanic datasets in the tropics, but also renew our interests in further investigating the role of atmosphere–ocean coupling on the MJO (Zhang et al. 2013). Different from most previous studies that carried out long-term free simulations (Waliser et al. 1999; Fu et al. 2003; Pegion and Kirtman 2008; Marshall et al. 2008), we take an alternative approach to study the impacts of air–sea coupling by carrying out initialized intraseasonal forecasting as some have done before (Vitart et al. 2007; Woolnough et al. 2007; Fu et al. 2008a; Kim et al. 2008; Seo et al. 2009; Kim et al. 2010; de Boisseson et al. 2012). This approach will take advantage of the latest-generation NCEP Climate Forecast System Reanalysis (CFSR; Saha et al. 2010), which has much better quality in terms of the representation of tropical intraseasonal variability (Wang et al. 2012) and potentially a better way to utilize the in situ measurements obtained from short-term field campaign, such as the DYNAMO/CINDY, to pinpoint the specific misrepresented model physical processes (Fu et al. 2013a; Williams et al. 2013).

In a recent study (Fu et al. 2013b), a series of intraseasonal hindcast experiments under different SST settings (Table 1) have been conducted for the extended DYNAMO/CINDY period (September 2011–March 2012). We have found that interactive air–sea coupling is able to improve the overall MJO forecasting skill by at least a week, when compared to the runs forced with persistent SST. The degree of skill advancement is similar to what we found for boreal summer monsoon intraseasonal predictability (Fu et al. 2007, 2008b). In the present study, more in-depth analysis will be carried out to (i) better understand the impacts of air–sea coupling on the initiation and propagation of the October and November MJO events (Fu et al. 2013b) and (ii) reveal the SST feedback processes by comparing the coupled and uncoupled forecasts. In particular, we will analyze the variations of the roles of air–sea coupling among the MJO events during the DYNAMO/CINDY field campaign.

TABLE 1. Hindcast experiments with the UH model under different SST settings. Initial conditions are the same for all the runs.

| Names of experiments | SST settings |
|---|---|
| CSST | Atmosphere–ocean coupled forecasts |
| Fcst_SST (or fsst) | Atmosphere-only forecasts driven by daily SST derived from the "csst" forecasts |
| Pers_SST (or psst) | Atmosphere-only forecasts driven by persistent SST |
| TMI_SST (or osst) | Atmosphere-only forecasts driven by observed daily TMI SST |

The remaining part of this paper is organized as follows. In section 2, we introduce the University of Hawaii (UH) coupled model and numerical experiments. Section 3 briefly documents the interactions between the MJO and underlying ocean during the DYNAMO/CINDY period and demonstrates that different air–sea coupling strengths are associated with the October and November MJO events. In a qualitative sense, the "coupling strength" is defined as the degree that the evolution of an individual MJO event relies on the coupling with underlying ocean. Quantitatively, the coupling strength can be measured as the difference of the MJO that is forced with observed SST forcing and that with persistent (or climatological) SST forcing.[1] In section 4, the major feedback processes from SST to November MJO evolutions in the UH model are revealed by comparing the coupled and uncoupled forecasts. Discussions and conclusions are given in section 5.

## 2. The model and experiments

This study primarily analyzes a series of intraseasonal forecasts carried out with the UH model during the DYNAMO/CINDY period. The UH model is an atmosphere–ocean coupled model (Fu et al. 2003)

[1] Like the "predictability," the "coupling strength" defined in this way is model dependent.

developed at International Pacific Research Center/School of Ocean and Earth Science and Technology (IPRC/SOEST), University of Hawai'i at Mānoa. The atmospheric component is a general circulation model (ECHAM4) with T106 (about 125 km) resolution that was originally developed at the Max Planck Institute for Meteorology, Germany (Roeckner et al. 1996). The Tiedtke–Nordeng mass flux scheme (Tiedtke 1989; Nordeng 1994) is used to represent the shallow, mid-level, and deep convections. The ocean component is an intermediate upper-ocean model developed at the University of Hawaii (Wang et al. 1995). It comprises a mixed layer and a thermocline layer with a horizontal resolution of 0.5° × 0.5°. The UH model carried out 45-day forecasts with 10 ensembles during the extended DYNAMO/CINDY period (September 2011–March 2012) every week initialized with final operational global analysis on 1° × 1° grid that was produced by NCEP, also known as FNL (available online at http://rda.ucar.edu/datasets/ds083.2/), which is almost the same as GDAS analysis (Kleist et al. 2009) but generated 1 h later. The perturbed initial conditions of the ensembles were generated by adding day-to-day root-mean-square differences of four prognostic variables ($u$, $v$, $t$, $q$) within the specific month onto the original initial conditions as in Waliser et al. (2003) and Fu et al. (2007). All modeling results presented in the following sections are from 10 ensemble means.

To quantify the degree that interactive air–sea coupling can contribute to the MJO fidelity, a suite of intraseasonal hindcast experiments was carried out. In addition to the set with interactive air–sea coupling, three more sets of atmosphere-only runs forced by different sea surface temperature settings are also carried out. The three SST sets include the persistent SST, daily SST generated from the air–sea coupled run, and daily SST from the observations. Detailed experimental design is given in Table 1. Since all four sets of forecasts have used the same initial conditions, the skill differences among them are attributed to the differences of the underlying SST settings. When measured with the Wheeler–Hendon index (Wheeler and Hendon 2004), the MJO forecast skill in the coupled run and the atmosphere-only run forced by forecasted daily SST are systematically higher (~1 week) than that forced with persistent SST. The run forced with observed daily SST has the highest forecast skill, which is about three weeks longer than that forced with persistent SST (Fu et al. 2013b). This result implies that the contribution of interactive air–sea coupling on MJO forecasting is between one and three weeks for the DYNAMO/CINDY period. In following sections, the impacts of air–sea coupling on the initiation and propagation of the October and November MJO events as well as the oceanic feedback processes will be investigated with the above hindcast outputs.

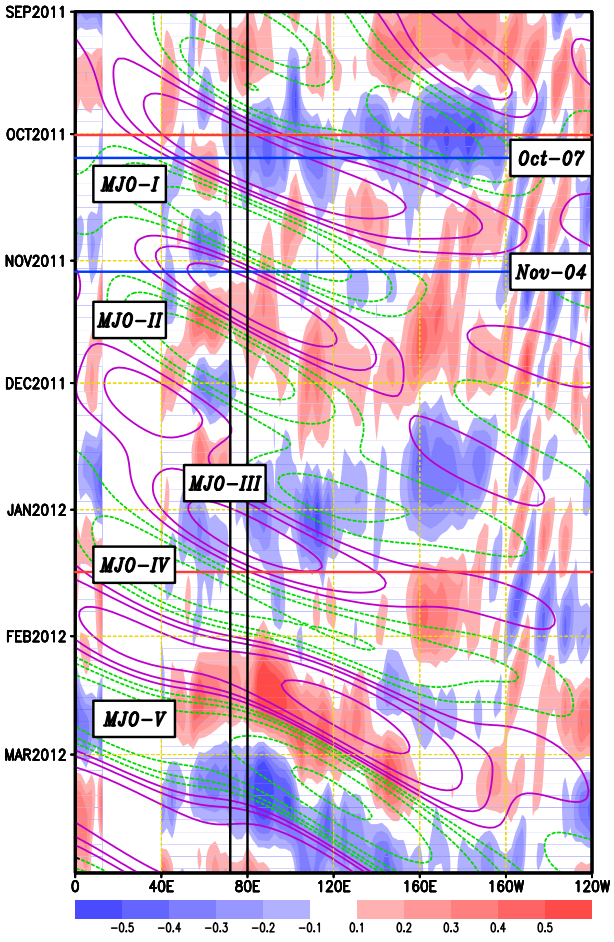


FIG. 1. Hovmöller diagram of the observed 30–90-day bandpass-filtered TMI SST (shading, °C) and MJO-projected NOAA OLR (contours of 2, 5, 10, 20, 30, and 40 W m$^{-2}$) anomalies averaged between 10°S and 10°N during the DYNAMO/CINDY period. Solid (dashed) lines represent positive (negative) values. The method used to extract the MJO is from Wheeler and Kiladis (1999).

## 3. Varying air–sea coupling strength for different MJO events

### a. *DYNAMO/CINDY observations*

The DYNAMO/CINDY[2] field campaign has been conducted in Indian Ocean from 1 October 2011 to 31 March 2012 with an intensive observing period (IOP) from 1 October 2011 to 15 January 2012. During the entire DYNAMO period, five MJO events are observed (Fig. 1) with the associated convective envelope over Indian Ocean, respectively, in the late October (MJO-I),

[2] More details on the DYNAMO and CINDY field campaigns can be found at http://www.eol.ucar.edu/projects/dynamo/ and http://www.jamstec.go.jp/iorgc/cindy/.

late November (MJO-II), late December (MJO-III), late January (MJO-IV),[3] and late February–early March (MJO-V). The first three MJO events occur during the DYNAMO IOP (Yoneyama et al. 2013). The definition of MJO initiation is still an open issue (e.g., Straub 2013) and the Indian Ocean is also not the only place MJO initiation can occur (Wang and Rui 1990a; Matthews 2008). Nevertheless, following the classic schematics of a MJO cycle depicted in Fig. 16 of Madden and Julian (1972), we take the definition of MJO initiation as the development of the convective envelope in the Indian Ocean associated with an eastward-propagating MJO cycle.

The MJOs-I, II, IV, and V are successive MJO events as defined by Matthews (2008), which are reinitiated over Indian Ocean by the circumglobal circulations associated with a preceding MJO event. The MJO-III is not well defined and also the weakest among the five MJOs. The MJO-III, initiated over the central Indian Ocean, was likely triggered by the westward-propagating mixed Rossby–gravity waves emanating from the Maritime Continent, which in turn were excited by the remnants of a tropical cyclone in the South China Sea (Kubota et al. 2012). Since coherent and robust SST fluctuations were observed in association with the two MJO events during the TOGA COARE field campaign (Anderson et al. 1996), it is interesting to see whether this is also the case during the DYNAMO/CINDY field campaign. The situation during recent campaign period seems rather complicated (Fig. 1). The active phase of the September MJO causes significant cooling over the eastern Indian Ocean, Maritime Continent, and western Pacific. The subsequent dry phase, however, does not produce coherent large-scale positive SST anomalies on its course eastward (Gottschalck et al. 2013; Johnson and Ciesielski 2013). This observational scenario suggests that the SST feedback has little impact on the evolution of the October MJO (MJO-I). It is also true for the late-December MJO (MJO-III) and late-January MJO (MJO-IV). On the other hand, for the November MJO (MJO-II) and late-February MJO (MJO-V), large-scale coherent positive SST anomalies systematically lead the onset and eastward propagation of the MJO convective envelopes as observed during the TOGA COARE period (Stephens et al. 2004) and illustrated in many previous modeling studies (e.g., Flatau et al. 1997; Wang and Xie 1998; Waliser et al. 1999; Marshall et al. 2008). The aforementioned observations and in situ measurements from the DYNAMO/CINDY field campaign (e.g., Johnson and Ciesielski 2013) actually suggest that the coupling strength between the MJO and underlying ocean varies event by event. This hypothesis will be examined in section 3b with our hindcast experiment outputs.

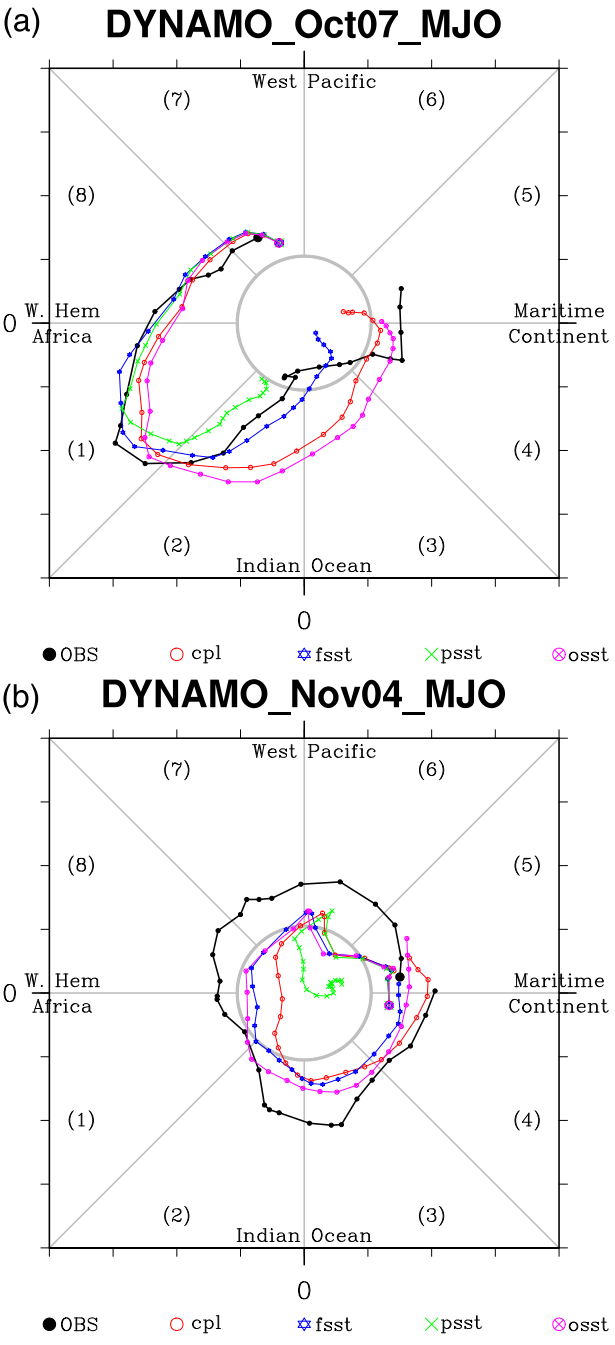


FIG. 2. Phase diagrams of the observed and forecasted Wheeler–Hendon index initialized on (a) 7 Oct and (b) 4 Nov 2011. The forecasts are carried out with UH model under different SST settings: the "OBS" for the observations, the "cpl," "fsst," "psst," and "osst" for the hindcasts from the coupled run, atmosphere-only runs forced by forecasted SST, persistent SST, and observed TMI daily SST (Table 1), respectively.

[3] This event is not classified as a significant MJO in some studies (e.g., Yoneyama et al. 2013).

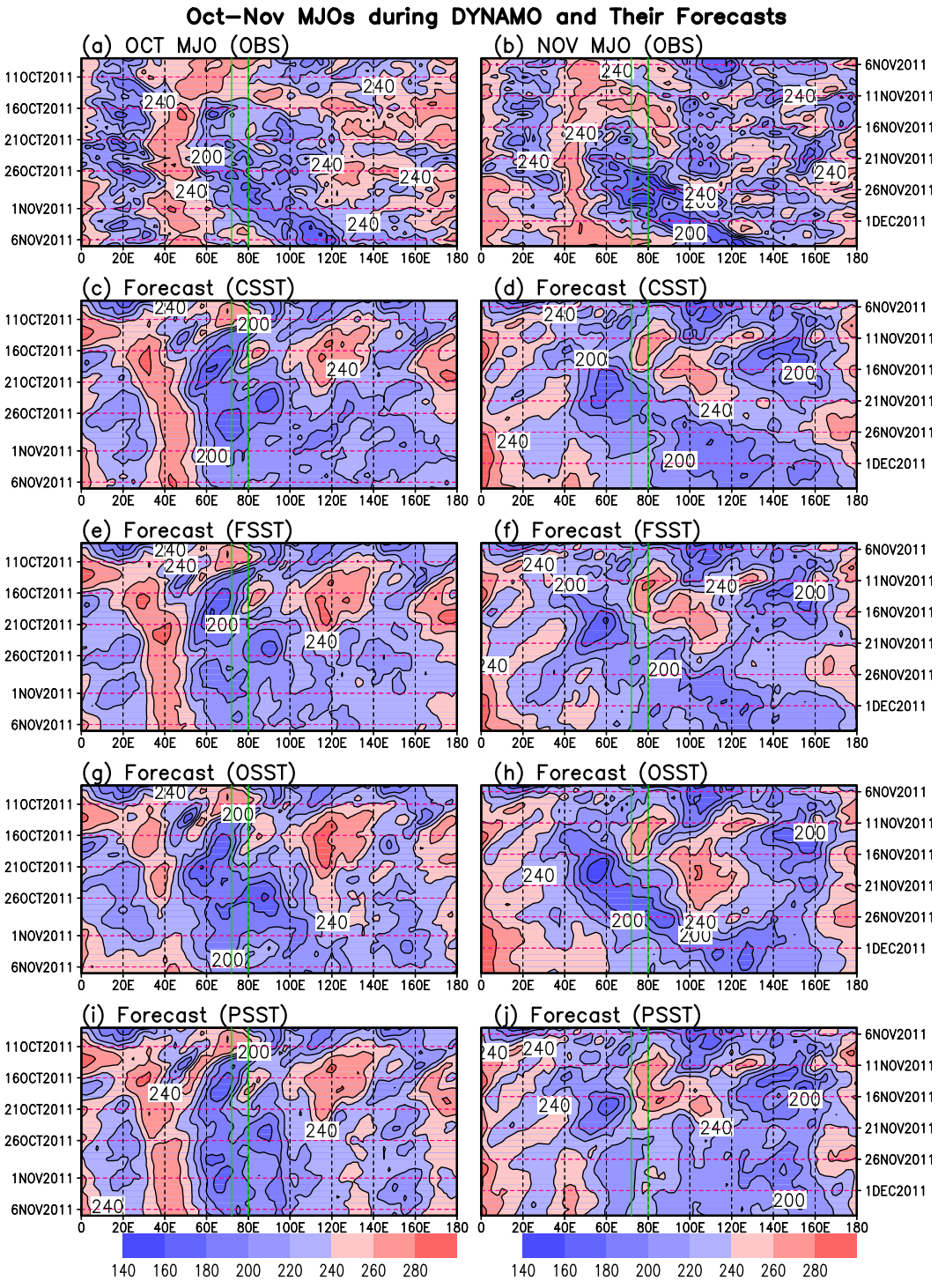


FIG. 3. Hovmöller diagrams of the observed NOAA OLR (W m$^{-2}$) and corresponding forecasts by the UH model coupled runs (CSST in Table 1) and atmosphere-only run driven by forecasted daily SST (FSST in Table 1), observed daily TMI SST (OSST in Table 1), and persistent SST (PSST in Table 1) averaged between 10°S and 10°N. The period from (left) 7 Oct to 7 Nov 2011 and (right) from 4 Nov to 4 Dec 2011.

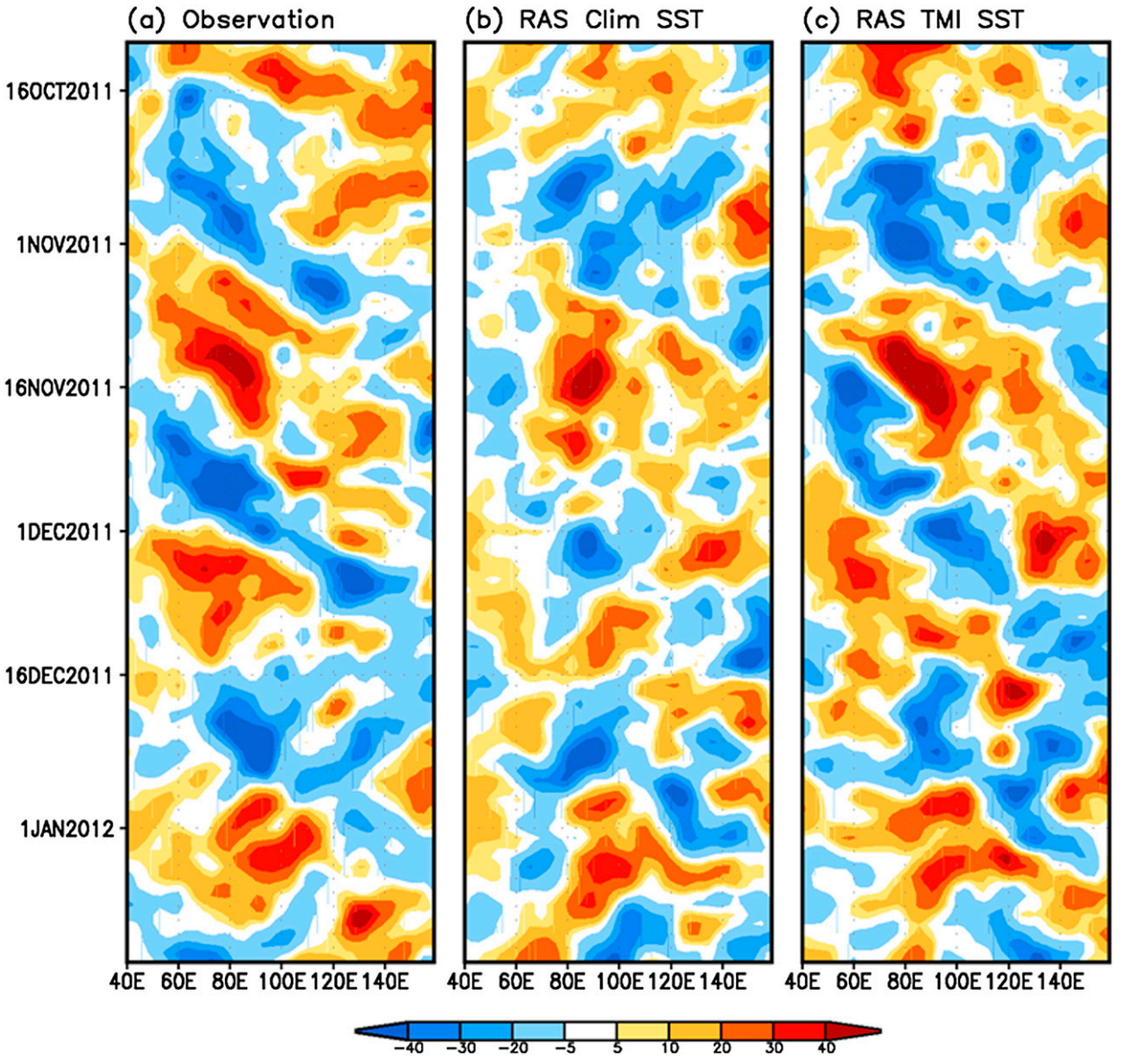


FIG. 4. Hovmöller diagrams of OLR anomalies from (a) the observations and two 11th day forecasts by a modified version of NCEP GFS atmosphere-only model forced with (b) climatological SST and (c) observed daily TMI SST.

### b. *Numerical modeling results*

The overall MJO forecast skill during the DYNAMO/CINDY period measured with the Wheeler–Hendon Real-time Multivariate MJO (RMM) index (Wheeler and Hendon 2004; Lin et al. 2008) in the active air–sea coupled runs is about one week longer (Fu et al. 2013b) than that forced with persistent SST. The observed changes in SST from event to event suggest the possibility that this skill advancement due to air–sea coupling is not uniformly distributed among all five MJO events. The impacts of SST feedback are expected to be larger for the November and February MJO events than that for the October, December, and January MJO events (Fig. 1).

To demonstrate this possibility, we take the forecasts initialized on 7 October and 4 November 2011 as two contrasting examples. Figures 2a and 2b show the phase diagrams of the observations and forecasts under different SST settings (Table 1) for a period of one month with two different initial conditions. For the case initialized on 7 October (Fig. 2a), the observed initial MJO is in phase 7 with a convective center in western Pacific (Figs. 3a and 4a). Regardless of what SST boundary conditions were used, all four forecasts capture the

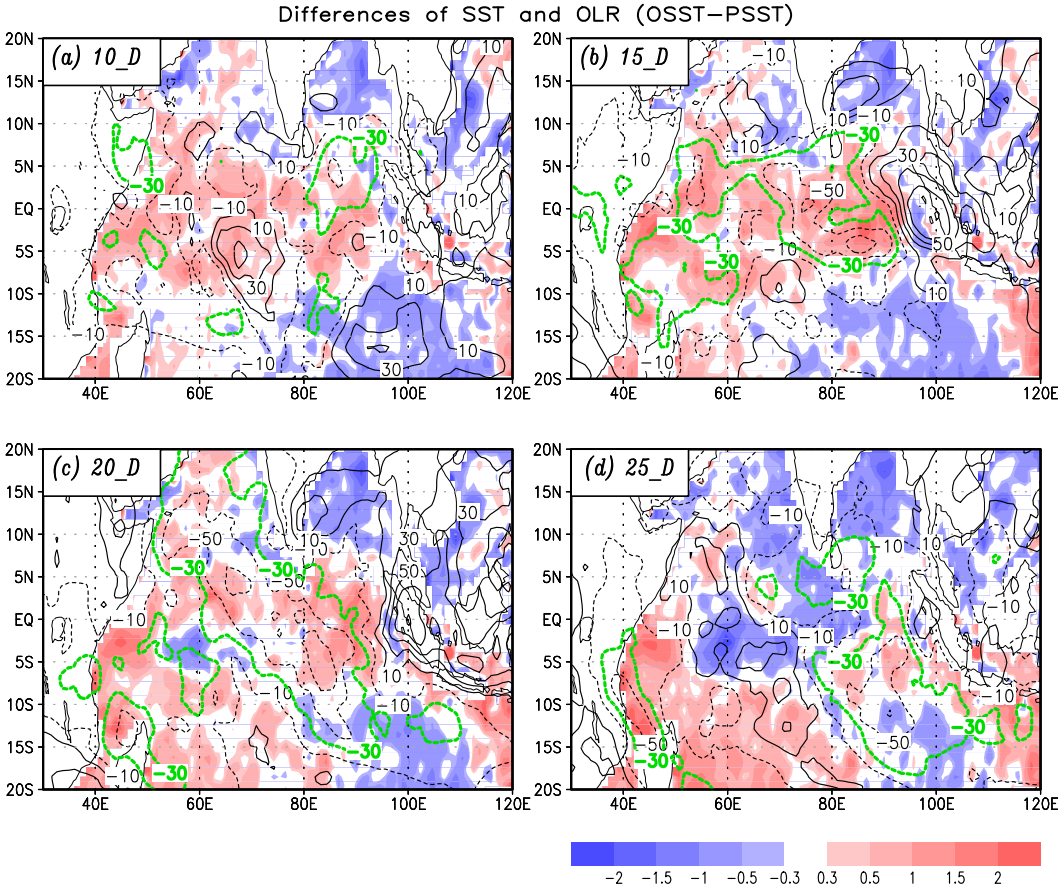


FIG. 5. The differences of SST (shading) and OLR (contours) between the forecasts driven with observed daily TMI SST (OSST in Table 1) and persistent SST (PSST in Table 1) at four different lead days: (a) 10, (b) 15, (c) 20, and (d) 25 days. Both forecasts are initialized on 4 Nov 2011.

eastward propagation and the reinitiation of the October MJO in the Indian Ocean. The MJO convective centers in all four runs reach phase 2 (Indian Ocean) after 14 days as in the observations (Fig. 2a).

For the case initialized on 4 November 2011, the MJO intensity in all four runs is weaker than that of the observations (Fig. 2b). During the first week, all four runs have very similar trajectory. After that, the MJO signal in the atmosphere-only run forced by persistent SST decays rapidly. The other three runs follow each other very well and all have similar propagation speed as in the observations. At the end of the 1-month forecasts, all three forecasts reach the Maritime Continent as in the observations (near the transition zone from phases 4 to 5). The much worse forecast in the persistent SST run than the other runs suggests that air–sea coupling is an indispensable factor for the initiation and propagation of the November MJO. The contrast between Figs. 2a and 2b does support that air–sea coupling plays a much more important role for the November MJO than for the October MJO.

The Wheeler–Hendon RMM index may be largely controlled by the large-scale baroclinic circulations rather than the MJO-related convection (e.g., Straub 2013). To examine the explicit impacts of air–sea coupling on MJO-related convection, the forecasted OLR evolution with initial conditions on 7 October and 4 November 2011 along with the corresponding observations are given in Figs. 3. For the October case, the observed MJO convection prevails over the DYNAMO/CINDY array from 21 October to 1 November 2011 (Fig. 3a) then steadily propagates to the western Pacific. All four runs (Figs. 3c,e,g,i) reproduce the MJO-associated rainy period over the array and subsequent eastward propagation. The run driven by persistent SST (Fig. 3i) tends to prolong the rainy period over the array with a slightly weaker eastward-propagating component than the other three runs. For the November case, the observed MJO convection reaches the DYNAMO/CINDY array around 21 November 2011 (Fig. 3b) then steadily propagates to the western Pacific. The three runs with intraseasonal SST variability in the boundary

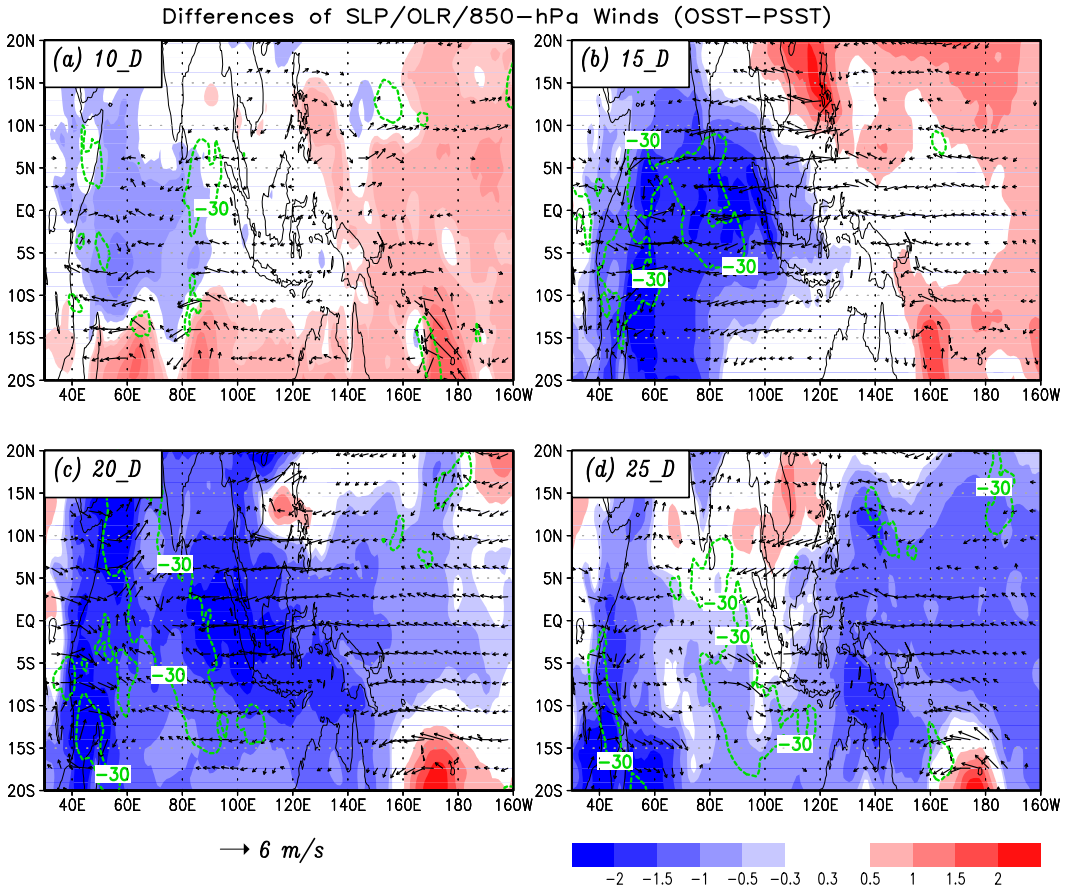


FIG. 6. The differences of sea level pressure (SLP in shading), OLR (contour of $-30\ \mathrm{W\ m^{-2}}$), and 850-hPa winds between the forecasts driven with observed daily TMI SST (OSST in Table 1) and persistent SST (PSST in Table 1) at four different lead days: (a) 10, (b) 15, (c) 20, and (d) 25 days. Both forecasts are initialized on 4 Nov 2011.

conditions (Figs. 3d,f,h) capture the initiation of November MJO in the Indian Ocean and the subsequent eastward propagation. The run forced with persistent SST (Fig. 3j), however, fails to reproduce the rainy period over the array and the subsequent eastward propagation. The obviously better reproducibility of the October MJO-related OLR (Fig. 3i) than that of the November MJO (Fig. 3j) under persistent SST condition also supports the fact that the SST feedback is more important for the November MJO than that for the October MJO.

Additional experiments with a modified version of the NCEP GFS atmosphere-only model[4] have also been carried out. Two sets of month-long forecasts initialized from each day of the DYNAMO-IOP period (1 October 2011–15 January 2012) are conducted. The only difference between these two sets of experiments is the underlying SST conditions: one with climatological SST and the other with observed daily Tropical Rainfall Measuring Mission (TRMM) Microwave Imager (TMI) SST. Both sets of experiments used the atmospheric initial conditions directly taken from NCEP CFSR (Saha et al. 2010). For each set of the experiments, four forecast runs are produced for each day at 0000, 0600, 1200, and 1800 UTC. The ensemble average based on the four forecast runs from each day is used to assess the impact of SSTs. Figure 4 compares the forecasted OLR anomalies at the 11th day of the two runs with the observations. It clearly shows that both the October and December MJO events can be largely reproduced even with climatological SST forcing, while the November MJO can only be reproduced when observed daily TMI SST is used as the underlying sea surface condition. This result further corroborates that the October MJO is largely controlled by atmospheric internal dynamics,

[4] The revised Simplified Arakawa–Schubert (SAS2) scheme (Han and Pan 2011) used in the operational NCEP GFS (the May 2011 version) has been replaced by a Relaxed Arakawa–Schubert (RAS) scheme (Moorthi and Suarez 1992). The modified version has much stronger MJO than the operational version (W. Q. Wang 2014, personal communication).

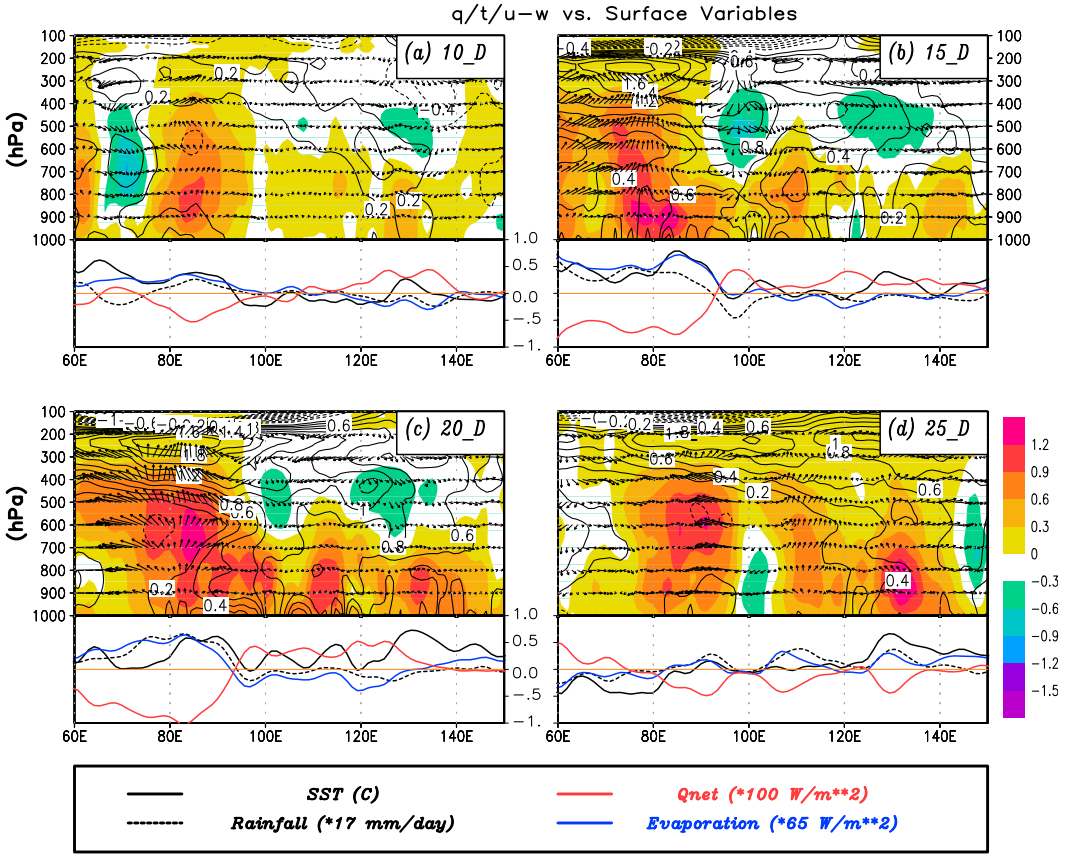


FIG. 7. (top part) The vertical structures of the differences of specific humidity (shading), temperature (contours), and circulations (arrows) between the forecasts driven with observed daily TMI SST (OSST in Table 1) and persistent SST (PSST in Table 1) averaged over 10°S and 10°N along with (bottom part) the differences of SST (°C), rainfall ($\times$17 mm day$^{-1}$), net surface heat flux ($\times$100 W m$^{-2}$), and surface evaporation ($\times$65 W m$^{-2}$) at four different lead days: (a) 10, (b) 15, (c) 20, and (d) 25 days. Both forecasts are initialized on 4 Nov 2011.

whereas the November MJO is strongly coupled to underlying ocean.

## 4. Processes through which SST feeds back to the MJO

Since the mean SST over the tropical Indo-Pacific sector is very high (with a large portion higher than 28°C), coherent SST perturbation in this region is expected to systematically modify the atmosphere above (Roxy 2014). When a robust positive SST anomaly is produced during the suppressed phase of the MJO [e.g., in front of the November MJO in Fig. 1 of this study and Fig. 5 in Johnson and Ciesielski (2013)], it tends to increase surface latent and sensible heat fluxes (Shinoda et al. 1998; Fu et al. 2006) and enhance boundary layer convergence through the Lindzen–Nigam mechanism (Lindzen and Nigam 1987; Fu and Wang 1999; Hsu and Li 2012). All these SST feedback processes are expected to improve model simulations of the MJO to some degree (Wang and Xie 1998; Waliser et al. 1999; Fu et al. 2008a; Marshall et al. 2008). However, the exact upward impact processes through which the aforementioned surface and boundary layer processes' changes can lead to better MJO simulations are still illusive. Since the successful reproduction of the November MJO in both the UH and NCEP models largely results from the underlying SST feedback (Figs. 2, 3, and 4), in the following analysis, we will look into the SST feedback processes in the UH model by comparing the forecasts initialized on 4 November with and without intraseasonal SST forcing.

Figure 5 shows the differences of SST and OLR between the OSST and PSST runs (Table 1) at different forecast lead times with initial conditions from 4 November 2011. Figure 6 shows the differences of the corresponding sea level pressure (SLP) and low-level winds. These differences represent the impacts of air–sea coupling on the initiation and propagation of the November MJO. As shown in Figs. 3h and 3j, both runs have very similar OLR in the first week. On day 10,

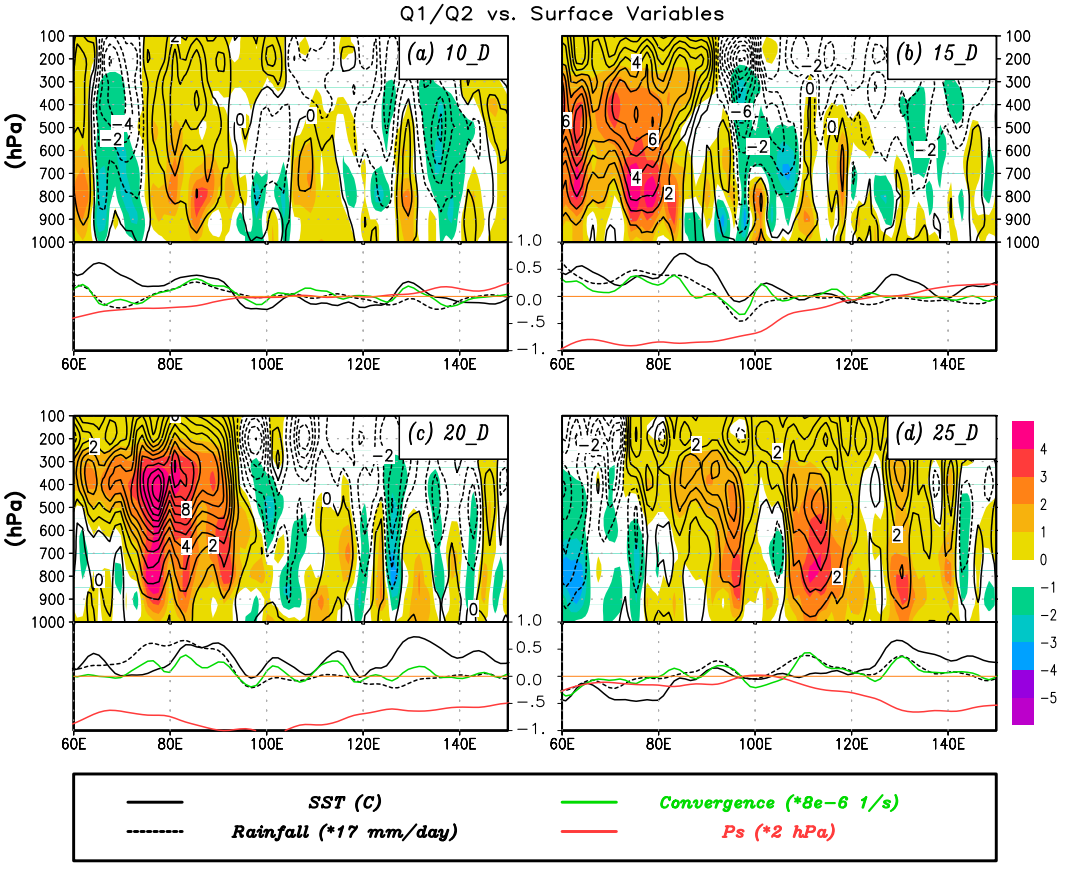


FIG. 8. (top part) The vertical structures of the differences of apparent moistening source $Q_2$ (shading) and apparent heating source $Q_1$ (contours) between the forecasts driven with observed daily TMI SST (OSST in Table 1) and persistent SST (PSST in Table 1) averaged over 10°S and 10°N along with (bottom part) the differences of SST (°C), rainfall ($\times 17$ mm day$^{-1}$), surface convergence ($\times 8 \times 10^{-6}$ s$^{-1}$), and surface pressure ($\times 2$ hPa) at four different lead days: (a) 10, (b) 15, (c) 20, and (d) 25 days. Both forecasts are initialized on 4 Nov 2011.

coherent positive SST anomalies appear across the equatorial Indian Ocean with enhanced convection (minus OLR anomaly $>30$ W m$^{-2}$) scattered around (Fig. 5a). Regional SLP is also systematically reduced (Fig. 6a). On day 15, the convective anomaly over the positive SST anomaly continues to enhance and become organized (Fig. 5b). A Kelvin–Rossby wave couplet is excited with two cyclonic Rossby wave–like disturbances straddling the equatorial western Indian Ocean along with the Kelvin wave response manifesting as an eastward-extended tongue of low SLP and easterly winds (Fig. 6b). Two anticyclonic circulations along with positive SLP anomalies are produced in subtropical regions of the western Pacific: resembling the Kelvin–Rossby wave couplet of the MJO three-dimensional structure first documented by Rui and Wang (1990) with available observations and reanalysis at that time. This result also supports the theoretical finding of Wang and Xie (1998) who suggested that air–sea coupling improves the representation of the MJO through destabilizing the Kelvin–Rossby wave couplet. Toward day 20, negative SST anomalies appear over the western Indian Ocean where enhanced convection gradually moves off the equator as Rossby wave–like disturbances (Figs. 5c and 6c). The Kelvin wave response is also enhanced and continues moving into western Pacific (Fig. 6c). On day 25, the equatorial Indian Ocean has largely cooled down except for the southwestern basin and a belt just west of Sumatra and Australia (Fig. 5d). Low SLP centers have also moved into the western Pacific (Fig. 6d).

To illustrate the upward impact processes of air–sea coupling on MJO evolution, Figs. 7 and 8 show the differences of the equatorial vertical structures of moisture, temperature, apparent heating source ($Q_1$), apparent moistening source ($Q_2$), and circulations along with some relevant surface variables between the OSST and PSST runs over the Indo-western Pacific sector. On

day 10 (Figs. 7a and 8a), in association with a positive SST anomaly around 90°E, surface evaporation and convergence are enhanced, which leads to intensified upward motion and tropospheric moistening (Fig. 7a). The peak level of the $Q_2$ is much lower than the $Q_1$ (Fig. 8a), which indicates the development of vigorous deep convection (Luo and Yanai 1984); this is a clear indication of a positive SST feedback intensifying MJO convection. The enhanced convection, on the other hand, reduces surface heat flux (Fig. 7a) by blocking downward solar radiation and increasing surface evaporation. On the eastern side of the enhanced deep convection, although some shallow cumuli pop up (Fig. 8a), the surface heat flux anomaly remains positive (means downward) and continues warming up the sea surface over the Maritime Continent and western Pacific (Fig. 7a). By day 15 (Figs. 7b and 8b), the convection near the array intensifies with increased upward motion and tropospheric moistening (Fig. 7b). The peak level of the $Q_2$ is gradually lifted upward (Fig. 8b), indicating that the contribution from stratiform rainfall is increased (Johnson and Young 1983). The covariability of upper-level heating and warming facilitates the production of eddy available potential energy (Fu and Wang 2009), which is essential to sustain the large-scale circulations associated with enhanced MJO convection (Hendon and Salby 1994; Mapes 2000; Kuang 2008).

By day 20, the rainfall anomaly near the DYNAMO/CINDY array reaches a maximum (Fig. 7c). The intensified upward motion, midtropospheric moistening, and upper-tropospheric warming are accompanied by the lower-tropospheric cooling and drying (Fig. 7c) similar to that of day 15 (Fig. 7b), likely reflecting the effects of intensified convective downdrafts (Lin and Johnson 1996). Large $Q_2$ peaks have moved up to the altitude of the $Q_1$ peaks (Fig. 8c), indicating that stratiform clouds play a dominant role during this period. An examination of the two forecasts clearly shows that the stratiform rainfall fraction (i.e., grid-scale precipitation in the model) for the OSST run is systematically larger than that for the PSST run after day-15 forecasts (Fig. 9). On the eastern side of the enhanced MJO convective envelope, shallow cumuli and congestus clouds pop up (Figs. 8a–c) due to the forcing of the positive SST anomaly and surface convergence originating from the interaction between the orography over the Maritime Continent and Kelvin wave–induced easterly winds [Fig. 6 in this manuscript, and Figs. 4 and 5 in Hsu and Lee (2005)]. These shallow and congestus clouds will not immediately develop into organized deep convection because of the prevalent subsidence induced by the enhanced convection near the array (Figs. 8a–c). Instead, they are largely detrained into the environment to moisten the boundary layer and lower troposphere (Figs. 7a–c), which is a process to buildup convective available potential energy (CAPE) and precondition the outbreak of deep convection. Toward day 25 (Figs. 7d and 8d), the enhanced convection over the western-central Indian Ocean has largely diminished, as does the associated subsidence on the eastern side. The release of the accumulated instability, therefore, leads to the outbreak of deep convection over the Maritime Continent and western Pacific, which is a manifestation of the eastward-propagating MJO.

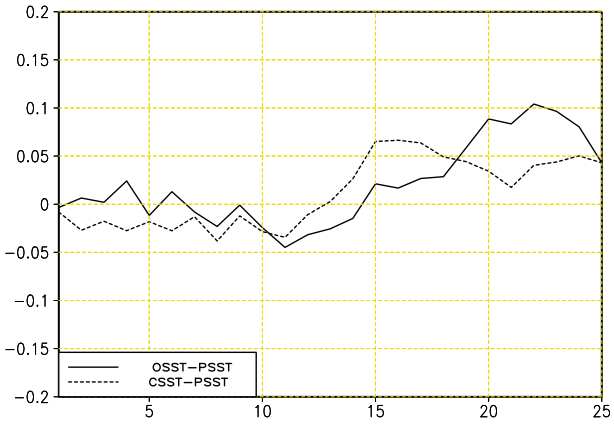


FIG. 9. Differences of stratiform rainfall fractions over (10°S–10°N, 60°–90°E) from three forecasts (OSST − PSST and CSST − PSST) initialized on 4 Nov 2011.

A similar situation is found for the differences between the air–sea coupled run (CSST in Table 1) and the persistent SST run (PSST in Table 1) as shown in Figs. 10 and 11. Compared to Figs. 7 and 8, the SST anomaly for the November MJO in our coupled model is much smaller, as are the atmospheric responses. The associated subsidence on the eastern side of the enhanced convection is also weaker. Rainfall differences around the array reach a maximum on day 15 (Figs. 10b and 11b) rather than day 20 in the (OSST − PSST) case (Figs. 7c and 8c). This is consistent with the time series of stratiform rainfall fraction differences given in Fig. 9, which shows that the stratiform rainfall fraction differences between the CSST run and the PSST run reach the maximum on 15 days. The weaker upper-level subsidence on the eastern side also shortens the CAPE accumulation time and allows for the faster outbreak of deep convection over the Maritime Continent and western Pacific. On day 20, enhanced convection center in this case has moved into the Maritime Continent (Figs. 10c and 11c), but still remains over the central Indian Ocean for the (OSST − PSST) case (Figs. 7c and 8c). This result indicates that the underestimated MJO–SST coupling strength in the CSST run over the Indian

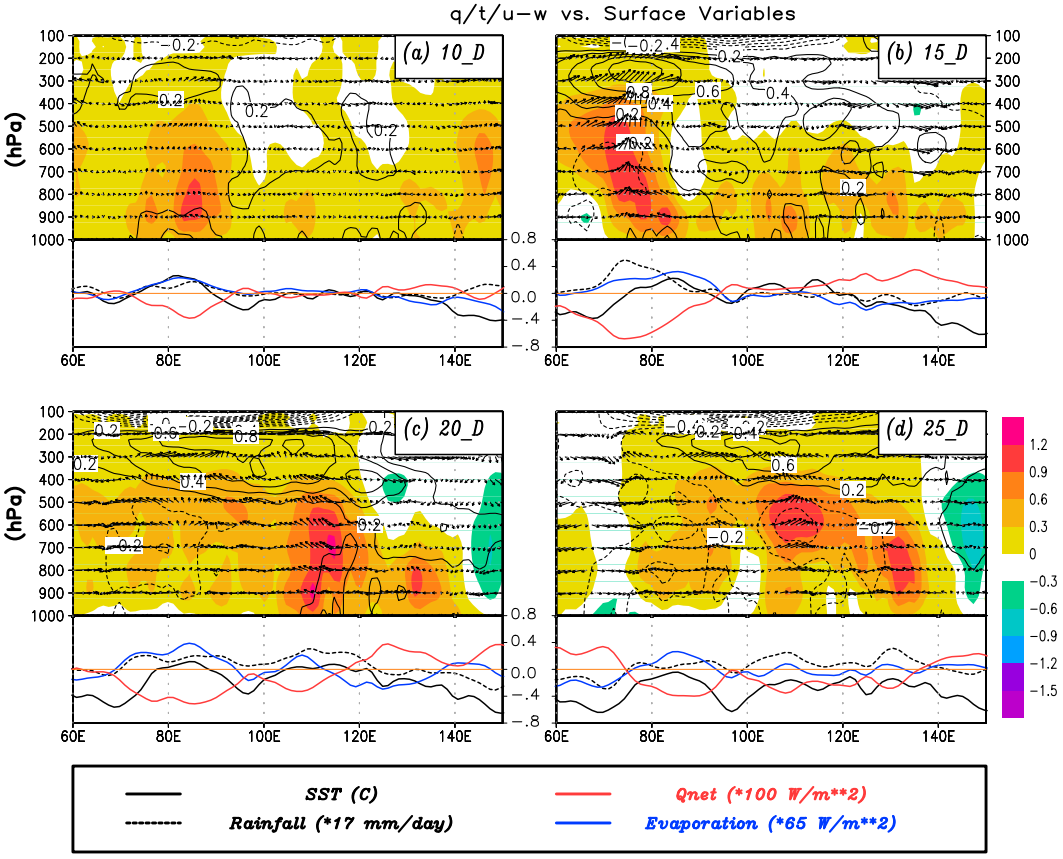


FIG. 10. (top part) The vertical structures of the differences of specific humidity (shading), temperature (contours), and circulations (arrows) between the coupled forecasts (CSST in Table 1) and the forecasts driven with persistent SST (PSST in Table 1) averaged over 10°S and 10°N along with (bottom part) the differences of SST (°C), rainfall ($\times$17 mm day$^{-1}$), surface evaporation ($\times$65 W m$^{-2}$), and net surface heat flux ($\times$100 W m$^{-2}$) at four different lead days: (a) 10, (b) 15, (c) 20, and (d) 25 days. Both forecasts are initialized on 4 Nov 2011.

Ocean leads to a faster MJO propagation than that with realistic intraseasonal SST forcing. The OLR evolution in Fig. 3 also shows that the MJO eastward propagation in the CSST run (Fig. 3d) is slightly faster than that in the observations (Fig. 3b) and the OSST run (Fig. 3h). It is also worth noting that the deep convection over the Maritime Continent in this case is largely supported by the surface convergence originating from the interaction between the orography and easterly winds induced by the Kelvin wave response (Figs. 11c,d) rather than from the local positive SST feedback.

## 5. Discussion and conclusions

### a. Discussion

One intriguing finding of the present study is that some MJO events do not have robust coherent SST variability associated with them, whereas the others do. This observational scenario suggests that the contribution of air–sea coupling to MJO evolution is case dependent. Why is this? For the two contrasting MJO events (the October and November MJO) observed during the DYNAMO/CINDY field campaign, this difference can be partly attributed to the shifts of background surface zonal winds (Li et al. 2008; Kanemaru and Masunaga 2014) over the equatorial Indian Ocean and western Pacific (Fig. 12). During the passage of the October MJO over the Indo-western Pacific sector (Figs. 12a,c), background easterly winds prevail in the entire region. When MJO-related convection reaches the Indian Ocean, the Kelvin wave response on the eastern side further intensifies the background winds and upward latent heat loss, which will offset the increased downward solar radiation. These two surface heat flux anomalies with opposite signs result in a negligible SST response in front of the MJO convection. On the other hand, during the passage of the November MJO, background zonal winds are changing to westerly (Figs. 12b,d). The easterly wind anomaly as a Kelvin

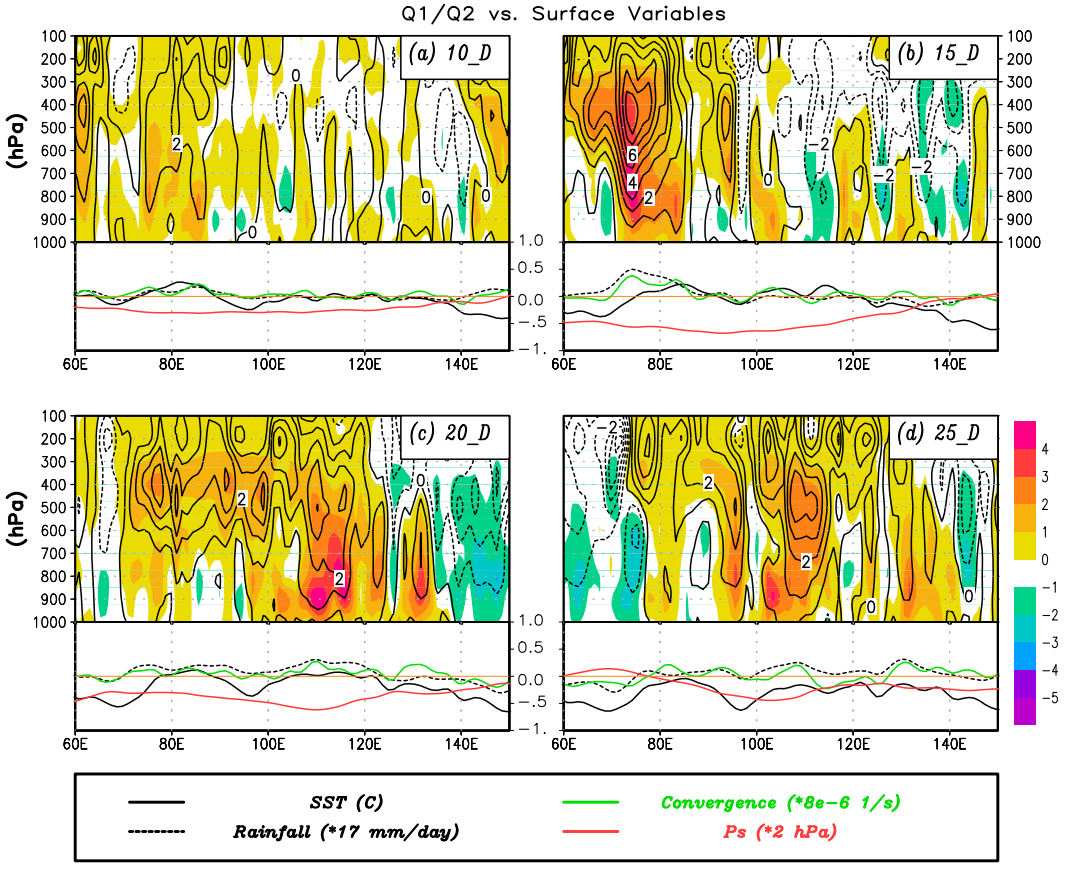


FIG. 11. (top part) The vertical structures of the differences of apparent moistening source $Q_2$ (shading) and apparent heating source $Q_1$ (contours) between the coupled forecasts (CSST in Table 1) and the forecasts driven with persistent SST (PSST in Table 1) averaged over 10°S and 10°N along with (bottom part) the differences of SST (°C), rainfall ($\times 17$ mm day$^{-1}$), surface convergence ($\times 8 \times 10^{-6}$ s$^{-1}$), and surface pressure ($\times 2$ hPa) at four different lead days: (a) 10, (b) 15, (c) 20, and (d) 25 days. Both forecasts are initialized on 4 Nov 2011.

wave response to the MJO convection reduces the background winds. As a result, coherent positive SST anomalies are produced by the combination of less upward latent heat loss and increased downward solar radiation. However, why no coherent SST anomalies were produced for the December and January MJO events are unclear. It may be due to the intensity of these two MJOs being too weak and the previous suppressed phases being too short. Future research with detailed analysis of the oceanic mixed layer heat budget is warranted to answer this question.

Which type of the MJO is more reproducible: the one largely controlled by atmospheric internal dynamics or the one strongly coupled to the underlying ocean? The results presented in Figs. 2 and 3 suggest that no clear predictability difference exists between them. For both the October and November MJO events, the UH coupled forecasts are able to capture their eastward propagations with reasonable amplitude beyond one month (Figs. 2 and 3). Future research is needed to examine this topic with more MJO events.

### b. Conclusions

A long-lasting issue faced by the MJO community is whether the MJO is primarily an atmospheric internal phenomenon (National Academy of Sciences 2010) or an atmosphere–ocean coupled system (Lau and Waliser 2011). This controversy originates from many conflicting results presented in the literature from a variety of theories [e.g., the wave-CISK, WISHE, frictional CISK, cloud–radiation feedback, moisture mode, multiscale interaction, and air–sea interaction, see a comprehensive review in Wang (2011)] to the state-of-the-art global general circulation model simulations. All theories, with either atmospheric internal dynamics only (e.g., Sobel and Maloney 2013) or air–sea coupling (e.g., Lau and Shen 1988; Hirst and Lau 1990; Wang and Xie 1998) are able to produce some kind of intraseasonal oscillation

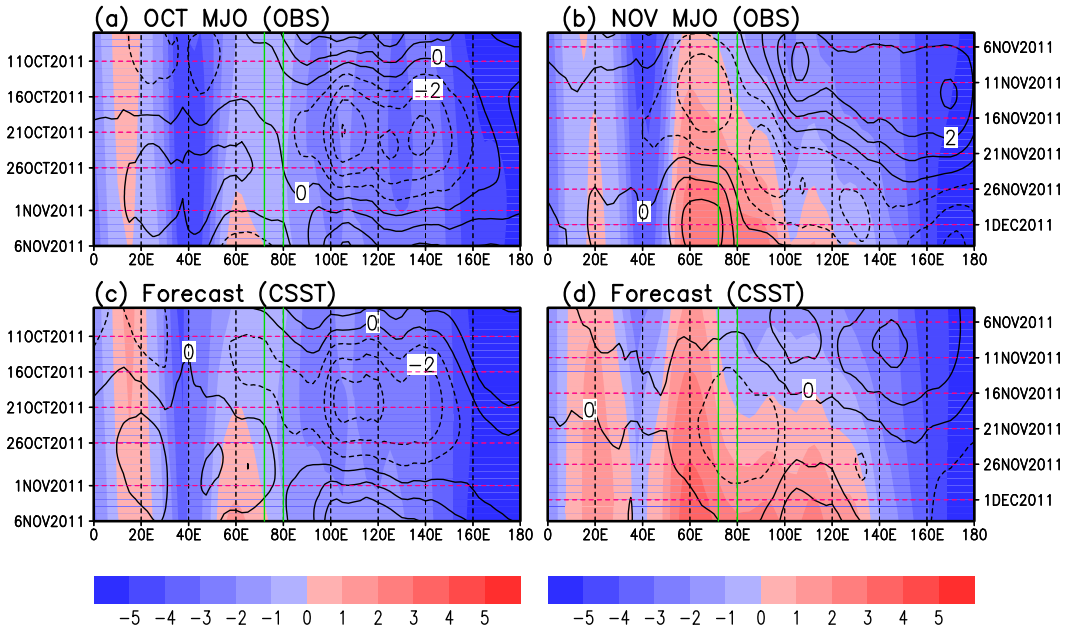


FIG. 12. Hovmöller diagrams of the 850-hPa background zonal wind (shading, m s$^{-1}$) and MJO-related perturbations (contours, m s$^{-1}$) along the equator (10°S–5°N) during the DYNAMO/CINDY period from the observations (OBS) for (a) the October MJO and (b) the November MJO, and from the coupled forecasts (CSST, Table 1) for (c) the October MJO and (d) the November MJO. The background zonal wind includes all variations with periods longer than 90 days.

that resembles the observed one. The coherent SST variability in association with two MJO events observed during TOGA COARE field campaign (November 1992–March 1993) further suggests the importance of air–sea coupling on the MJO dynamics. Although many numerical modeling studies have shown that air–sea coupling improves the simulations of the MJO, our overall capability of simulating the MJO in coupled models (e.g., CMIP3 and CMIP5) is still very poor (e.g., Hung et al. 2013). On the other hand, a global cloud-system-resolving atmosphere-only model without ocean coupling [i.e., the Nonhydrostatic Icosahedral Atmospheric Model (NICAM); Satoh et al. 2005] is able to reproduce an MJO event well (Miura et al. 2007; Liu et al. 2009). This successful case study also suggests that some MJO events are largely controlled by atmospheric internal dynamics.

During the DYNAMO/CINDY period, the atmosphere–ocean variations depicted in this study and from in situ measurements (e.g., Johnson and Ciesielski 2013; Moum et al. 2014) reveal the complexity in terms of the MJO interactions with underlying ocean. Five MJO events are observed during this period; however, coherent robust SST anomalies are associated only with two of them (Fig. 1). The October and November MJO events are two contrasting cases in this sense. For the October MJO, little coherent positive SST anomaly was observed in front of the convection. On the other hand, large-scale robust SST anomalies are observed to systematically lead the initiation, development, and propagation of the November MJO. This observational picture suggests that the October MJO is basically controlled by atmospheric internal dynamics, whereas the November MJO is strongly coupled to the underlying ocean.

To test this hypothesis, a series of initialized intraseasonal forecasts with different SST settings have been carried out for these two MJO events. For the October MJO, all forecasts initialized on 7 October 2011 with interactive air–sea coupling, atmosphere-only runs forced with persistent SST, and daily SST from the coupled run and the observations are able to capture the initiation over the DYNAMO/CINDY array and subsequent eastward propagation to some degree (Figs. 2a and 3a,c,e,g,i). One major difference among the forecasts is the amplitude. The forecasts with intraseasonal SST forcing have larger MJO amplitude than those with persistent SST. For the November MJO, the three forecasts with intraseasonal SST forcing are apparently distinguished from the forecast driven with persistent SST (Figs. 2b and 3b,d,f,h,j). In the persistent SST run, the MJO signal is similar to the other three runs only in the first week. After that, the MJO basically disappears in the forecast. These sensitivity experiments clearly demonstrate that the October MJO event is largely controlled by atmospheric internal dynamics, while the November MJO is strongly coupled with

the underlying ocean. Additional experiments with the NCEP GFS atmosphere-only model also corroborate the above findings.

Further analysis of the November MJO forecasts with and without intraseasonal SST forcing (the OSST, CSST, and PSST runs in Table 1) has been carried out to reveal the SST feedback processes in the UH model. The primary path of SST feedback in this model is through enhancing the Kelvin–Rossby wave couplet (Fig. 6) as suggested in a previous theoretical study of Wang and Xie (1998). The more detailed upward impacts from the SST anomaly to the November MJO evolution are illustrated with the vertical structures of the moisture, temperature, apparent heating profile ($Q_1$), and apparent moistening profile ($Q_2$) along with some relevant surface variables (Figs. 7, 8, 10, and 11). The positive SST anomaly in the Indian Ocean enhances surface evaporation and convergence, thus the local deep convection (Figs. 7 and 10). It also prolongs the positive feedback between the convection and large-scale circulation, therefore, facilitating the development of stratiform rainfall that produces large-eddy available potential energy to maintain the MJO-related large-scale circulations.

The overturning circulation associated with the major convection of the MJO in the Indian Ocean intensifies the upper-level subsidence over the Maritime Continent and western Pacific. Along with the lower-tropospheric moistening and heating forced by local positive SST anomalies and surface convergence induced by the interaction between the orography and easterly winds of the Kelvin wave response, the convectively available potential energy (CAPE) is accumulated over the Maritime Continent and western Pacific. Once the sea surface cools off and the convection fades away in the Indian Ocean, the associated weakening of the upper-level subsidence on the eastern side allows for the outbreak of deep convection over the Maritime Continent and western Pacific, leading to the eastward propagation of the November MJO.

*Acknowledgments.* This work was sponsored by NOAA Grants NA11OAR4310096 and NA10OAR4310247, NSF Grant AGS-1005599, and by the Japan Agency for Marine-Earth Science and Technology (JAMSTEC) and NOAA through their supports of the IPRC. Additional supports are from APEC Climate Center, GRL Grant MEST 2011-0021927, CMA Project GYHY201206016, and NSFC41005057.

## REFERENCES

Anderson, S. P., R. A. Weller, and R. Lukas, 1996: Surface buoyancy forcing and the mixed layer in the western Pacific warm pool: Observation and 1D model results. *J. Climate,* **9,** 3056–3085, doi:10.1175/1520-0442(1996)009<3056:SBFATM>2.0.CO;2.

Araligidad, N. M., and E. D. Maloney, 2008: Wind-driven latent heat flux and the intraseasonal oscillation. *Geophys. Res. Lett.,* **35,** L04815, doi:10.1029/2007GL032746.

Brunet, G., and Coauthors, 2010: Collaboration of the weather and climate communities to advance subseasonal to seasonal prediction. *Bull. Amer. Meteor. Soc.,* **91,** 1397–1406, doi:10.1175/2010BAMS3013.1.

Chang, C.-P., and H. Lim, 1988: Kelvin wave-CISK: A possible mechanism for the 30–50 day oscillations. *J. Atmos. Sci.,* **45,** 1709–1720, doi:10.1175/1520-0469(1988)045<1709:KWCAPM>2.0.CO;2.

Chou, C., and Y.-C. Hsueh, 2010: Mechanisms of northward-propagating intraseasonal oscillation—A comparison between the Indian Ocean and the western North Pacific. *J. Climate,* **23,** 6624–6640, doi:10.1175/2010JCLI3596.1.

de Boisseson, E., M. A. Balmaseda, F. Vitart, and K. Mogensen, 2012: Impact of the sea surface temperature forcing on hindcasts of Madden–Julian oscillation events during the ECMWF model. *Ocean Sci.,* **8,** 1071–1084, doi:10.5194/os-8-1071-2012.

Donald, A., H. Meinke, B. Power, A. de H. N. Maia, M. C. Wheeler, N. White, R. C. Stone, and J. Ribbe, 2006: Near-global impact of the Madden-Julian Oscillation on rainfall. *Geophys. Res. Lett.,* **33,** L09704, doi:10.1029/2005GL025155.

Emanuel, K. A., 1987: Air-sea interaction model of intraseasonal oscillations in the Tropics. *J. Atmos. Sci.,* **44,** 2324–2340, doi:10.1175/1520-0469(1987)044<2324:AASIMO>2.0.CO;2.

Flatau, M., P. J. Flatau, P. Phoebus, and P. P. Niiler, 1997: The feedback between equatorial convection and local radiative and evaporative processes: The implication for intraseasonal oscillations. *J. Atmos. Sci.,* **54,** 2373–2386, doi:10.1175/1520-0469(1997)054<2373:TFBECA>2.0.CO;2.

Fu, X., and B. Wang, 1999: On the role of longwave radiation and boundary layer thermodynamics on forcing tropical surface winds. *J. Climate,* **12,** 1049–1069, doi:10.1175/1520-0442(1999)012<1049:TROLRA>2.0.CO;2.

——, and ——, 2004: Differences of boreal-summer intraseasonal oscillations simulated in an atmosphere–ocean coupled model and an atmosphere-only model. *J. Climate,* **17,** 1263–1271, doi:10.1175/1520-0442(2004)017<1263:DOBSIO>2.0.CO;2.

——, and ——, 2009: Critical roles of the stratiform rainfall in sustaining the Madden–Julian oscillation: GCM experiments. *J. Climate,* **22,** 3939–3959, doi:10.1175/2009JCLI2610.1.

——, ——, T. Li, and J. P. McCreary, 2003: Coupling between northward-propagating intraseasonal oscillations and sea surface temperature in the Indian Ocean. *J. Atmos. Sci.,* **60,** 1733–1753, doi:10.1175/1520-0469(2003)060<1733:CBNIOA>2.0.CO;2.

——, ——, and L. Tao, 2006: Satellite data revealed the 3-D moisture structure of tropical intraseasonal oscillation and its coupling with underlying ocean. *Geophys. Res. Lett.,* **33,** L03705, doi:10.1029/2005GL025074.

——, ——, D. E. Waliser, and L. Tao, 2007: Impact of atmosphere–ocean interaction on the predictability of monsoon intraseasonal oscillation. *J. Atmos. Sci.,* **64,** 157–174, doi:10.1175/JAS3830.1.

——, ——, Q. Bao, P. Liu, and B. Yang, 2008a: Experimental dynamical forecast of an MJO event observed during TOGA-COARE period. *Atmos. Oceanic Sci. Lett.,* **1,** 24–28.

——, B. Yang, Q. Bao, and B. Wang, 2008b: Sea surface temperature feedback extends the predictability of tropical intraseasonal oscillation. *Mon. Wea. Rev.,* **136,** 577–597, doi:10.1175/2007MWR2172.1.

——, B. Wang, J.-Y. Lee, W. Q. Wang, and L. Gao, 2011: Sensitivity of dynamical intraseasonal prediction skills to different initial conditions. *Mon. Wea. Rev.,* **139,** 2572–2592, doi:10.1175/2011MWR3584.1.

——, J.-Y. Lee, B. Wang, W. Q. Wang, and F. Vitart, 2013a: Intraseasonal forecasting of the Asian summer monsoon in four operational and research models. *J. Climate,* **26,** 4186–4203, doi:10.1175/JCLI-D-12-00252.1.

——, ——, P.-C. Hsu, H. Taniguchi, B. Wang, W. Q. Wang, and S. Weaver, 2013b: Multi-model MJO forecasting during DYNAMO/CINDY period. *Climate Dyn.,* **41,** 1067–1081, doi:10.1007/s00382-013-1859-9.

Gottschalck, J., P. E. Roundy, C. J. Schreck, A. Vintzileos, and C. D. Zhang, 2013: Large-scale atmospheric and oceanic conditions during the 2011–12 DYNAMO field campaign. *Mon. Wea. Rev.,* **141,** 4173–4196, doi:10.1175/MWR-D-13-00022.1.

Han, J., and H.-L. Pan, 2011: Revision of convection and vertical diffusion schemes in the NCEP Global Forecast System. *Wea. Forecasting,* **26,** 520–533, doi:10.1175/WAF-D-10-05038.1.

Han, W. Q., D. L. Yuan, W. T. Liu, and D. J. Hakides, 2007: Intraseasonal variability of Indian Ocean sea surface temperature during boreal winter: Madden-Julian Oscillation versus submonthly forcing and processes. *J. Geophys. Res.,* **112,** C04001, doi:10.1029/2006JC003791.

Hendon, H. H., 2000: Impact of air–sea coupling on the Madden–Julian oscillation in a general circulation model. *J. Atmos. Sci.,* **57,** 3939–3952, doi:10.1175/1520-0469(2001)058<3939:IOASCO>2.0.CO;2.

——, and M. L. Salby, 1994: The life cycle of the Madden–Julian Oscillation. *J. Atmos. Sci.,* **51,** 2225–2237, doi:10.1175/1520-0469(1994)051<2225:TLCOTM>2.0.CO;2.

Hirst, A., and K.-M. Lau, 1990: Intraseasonal and interannual oscillations in coupled ocean–atmosphere models. *J. Climate,* **3,** 713–725, doi:10.1175/1520-0442(1990)003<0713:IAIOIC>2.0.CO;2.

Hoskins, B., 2013: The potential for skill across the range of the seamless weather-climate prediction problem: A stimulus for our science. *Quart. J. Roy. Meteor. Soc.,* **139,** 573–584, doi:10.1002/qj.1991.

Hsu, H. H., and M. Y. Lee, 2005: Topographic effects on the eastward propagation and initiation of the Madden–Julian Oscillation. *J. Climate,* **18,** 795–809, doi:10.1175/JCLI-3292.1.

Hsu, P.-C., and T. Li, 2012: Role of the boundary layer moisture asymmetry in causing the eastward propagation of the Madden–Julian oscillation. *J. Climate,* **25,** 4914–4931, doi:10.1175/JCLI-D-11-00310.1.

Hung, M., J. Lin, W. Q. Wang, D. Kim, T. Shinoda, and S. Weaver, 2013: MJO and convectively coupled equatorial waves simulated by CMIP5 climate models. *J. Climate,* **26,** 6185–6214, doi:10.1175/JCLI-D-12-00541.1.

Johnson, R. H., and G. S. Young, 1983: Heat and moisture budgets of tropical mesoscale anvil clouds. *J. Atmos. Sci.,* **40,** 2138–2147, doi:10.1175/1520-0469(1983)040<2138:HAMBOT>2.0.CO;2.

——, and P. E. Ciesielski, 2013: Structure and properties of Madden–Julian oscillations deduced from DYNAMO sounding arrays. *J. Atmos. Sci.,* **70,** 3157–3179, doi:10.1175/JAS-D-13-065.1.

——, T. M. Rickenbach, S. A. Rutledge, P. E. Ciesielski, and W. H. Schubert, 1999: Trimodal characteristics of tropical convection. *J. Climate,* **12,** 2397–2418, doi:10.1175/1520-0442(1999)012<2397:TCOTC>2.0.CO;2.

Jones, C., and B. C. Weare, 1996: The role of low-level moisture convergence and ocean latent heat fluxes in the Madden and Julian Oscillation: An observational analysis using ISCCP data and ECMWF analyses. *J. Climate,* **9,** 3086–3104, doi:10.1175/1520-0442(1996)009<3086:TROLLM>2.0.CO;2.

Kanemaru, K., and H. Masunaga, 2014: The potential roles of background surface wind in the SST variability associated with intraseasonal oscillations. *J. Climate,* **27,** 7053–7068, doi:10.1175/JCLI-D-13-00774.1.

Kikuchi, K., and Y. N. Takayabu, 2004: The development of organized convection associated with the MJO during TOGA COARE IOP: Trimodal characteristics. *Geophys. Res. Lett.,* **31,** L10101, doi:10.1029/2004GL019601.

——, and B. Wang, 2010: Spatiotemporal wavelet transform and the multiscale behavior of the Madden–Julian oscillation. *J. Climate,* **23,** 3814–3834, doi:10.1175/2010JCLI2693.1.

Kim, H. M., C. D. Hoyos, P. J. Webster, and I. S. Kang, 2008: Sensitivity of MJO simulation and predictability to sea surface temperature variability. *J. Climate,* **21,** 5304–5317, doi:10.1175/2008JCLI2078.1.

——, ——, ——, and ——, 2010: Ocean-atmosphere coupling and the boreal winter MJO. *Climate Dyn.,* **35,** 771–784, doi:10.1007/s00382-009-0612-x.

Kleist, D. T., D. F. Parrish, J. C. Derber, R. Treadon, W.-S. Wu, and S. Lord, 2009: Introduction of the GSI into the NCEP Global Data Assimilation System (GDAS). *Wea. Forecasting,* **24,** 1691–1705, doi:10.1175/2009WAF2222201.1.

Krishnamurti, T. N., D. K. Oosterhof, and A. V. Mehta, 1988: Air–sea interaction on the time scale of 30 to 50 days. *J. Atmos. Sci.,* **45,** 1304–1322, doi:10.1175/1520-0469(1988)045<1304:AIOTTS>2.0.CO;2.

——, M. Subramaniam, G. Daughenbaugh, D. Oosterhof, and J. H. Xue, 1992: One-month forecasts of wet and dry spells of the monsoon. *Mon. Wea. Rev.,* **120,** 1191–1223, doi:10.1175/1520-0493(1992)120<1191:OMFOWA>2.0.CO;2.

Kuang, Z. M., 2008: A moisture-stratiform instability for convectively coupled waves. *J. Atmos. Sci.,* **65,** 834–854, doi:10.1175/2007JAS2444.1.

Kubota, H., K. Yoneyama, and H. Jun-Ichi, 2012: Contribution of tropical cyclone for the preconditioning of the Madden-Julian Oscillation during CINDY2011. *2012 Fall Meeting,* San Francisco, CA, Amer. Geophys. Union, Abstract A13A-0213.

Lau, K. M., and L. Peng, 1987: Origin of low frequency (intraseasonal) oscillations in the tropical atmosphere. Part I: Basic theory. *J. Atmos. Sci.,* **44,** 950–972, doi:10.1175/1520-0469(1987)044<0950:OOLFOI>2.0.CO;2.

——, and S. Shen, 1988: On the dynamics of intraseasonal oscillations and ENSO. *J. Atmos. Sci.,* **45,** 1781–1797, doi:10.1175/1520-0469(1988)045<1781:OTDOIO>2.0.CO;2.

——, and D. E. Waliser, Eds., 2011: *Intraseasonal Variability of the Atmosphere–Ocean Climate System.* 2nd ed. Springer, 613 pp.

Lau, N.-C., I. M. Held, and J. D. Neelin, 1988: The Madden–Julian Oscillation in an idealized GCM model. *J. Atmos. Sci.,* **45,** 3810–3832, doi:10.1175/1520-0469(1988)045<3810:TMJOIA>2.0.CO;2.

Li, T., F. Tam, X. Fu, T.-J. Zhou, and W.-J. Zhu, 2008: Causes of the intraseasonal SST variability in the tropical Indian Ocean. *Atmos. Oceanic Sci. Lett.,* **1,** 18–23.

Lin, H., G. Brunet, and J. Derome, 2008: Forecast skill of the Madden–Julian Oscillation in two Canadian atmospheric models. *Mon. Wea. Rev.,* **136,** 4130–4149, doi:10.1175/2008MWR2459.1.

Lin, J.-L., and R. H. Johnson, 1996: Heating, moistening, and rainfall over the western Pacific warm pool during TOGA

COARE. *J. Atmos. Sci.,* **53,** 3367–3383, doi:10.1175/1520-0469(1996)053<3367:HMAROT>2.0.CO;2.

——, and Coauthors, 2006: Tropical intraseasonal variability in 14 IPCC AR4 climate models. Part I: Convective signals. *J. Climate,* **19,** 2665–2690, doi:10.1175/JCLI3735.1.

Lindzen, R. S., and S. Nigam, 1987: On the role of sea surface temperature gradients in forcing low-level winds and convergence in the tropics. *J. Atmos. Sci.,* **44,** 2418–2436, doi:10.1175/1520-0469(1987)044<2418:OTROSS>2.0.CO;2.

Liu, P., and Coauthors, 2009: An MJO simulated by the NICAM at 14- and 7-km resolutions. *Mon. Wea. Rev.,* **137,** 3254–3268, doi:10.1175/2009MWR2965.1.

Luo, H., and M. Yanai, 1984: The large-scale circulation and heat sources over the Tibetan Plateau and surrounding areas during the early summer of 1979. Part II: Heat and moisture budgets. *Mon. Wea. Rev.,* **112,** 966–989, doi:10.1175/1520-0493(1984)112<0966:TLSCAH>2.0.CO;2.

Madden, R. A., and P. R. Julian, 1971: Detection of a 40-50-day oscillation in the zonal wind in the tropical Pacific. *J. Atmos. Sci.,* **28,** 702–708, doi:10.1175/1520-0469(1971)028<0702:DOADOI>2.0.CO;2.

——, and ——, 1972: Description of global-scale circulation cells in the tropics with a 40-50 day period. *J. Atmos. Sci.,* **29,** 1109–1123, doi:10.1175/1520-0469(1972)029<1109:DOGSCC>2.0.CO;2.

Maloney, E. D., and A. H. Sobel, 2004: Surface fluxes and ocean coupling in the tropical intraseasonal oscillation. *J. Climate,* **17,** 4368–4386, doi:10.1175/JCLI-3212.1.

Mapes, B. E., 2000: Convective inhabitation, subgrid-scale triggering energy, and stratiform instability in a toy tropical wave model. *J. Atmos. Sci.,* **57,** 1515–1535, doi:10.1175/1520-0469(2000)057<1515:CISSTE>2.0.CO;2.

Marshall, A. G., O. Alves, and H. H. Hendon, 2008: An enhanced moisture convergence–evaporation feedback mechanism for MJO air–sea interaction. *J. Atmos. Sci.,* **65,** 970–986, doi:10.1175/2007JAS2313.1.

Matsueda, M., and H. Endo, 2011: Verification of medium-range MJO forecasts with TIGGE. *Geophys. Res. Lett.,* **38,** L11801, doi:10.1029/2011GL047480.

Matthews, A. J., 2008: Primary and successive events in the Madden-Julian oscillation. *Quart. J. Roy. Meteor. Soc.,* **134,** 439–453, doi:10.1002/qj.224.

Miura, H., M. Satoh, T. Nasuno, A. T. Noda, and K. Oouchi, 2007: A Madden-Julian oscillation event realistically simulated by a global cloud-resolving model. *Science,* **318,** 1763–1765, doi:10.1126/science.1148443.

Moncrieff, M. W., D. E. Waliser, M. J. Miller, M. E. Shapiro, G. Asrar, and J. Caughey, 2012: Multiscale convective organization and the YOTC Virtual Global Field Campaign. *Bull. Amer. Meteor. Soc.,* **93,** 1171–1187, doi:10.1175/BAMS-D-11-00233.1.

Moorthi, S., and M. J. Suarez, 1992: Relaxed Arakawa–Schubert: A parameterization of moist convection for general circulation models. *Mon. Wea. Rev.,* **120,** 978–1002, doi:10.1175/1520-0493(1992)120<0978:RASAPO>2.0.CO;2.

Moum, J. N., and Coauthors, 2014: Air–sea interactions from westerly wind bursts during the November 2011 MJO in the Indian Ocean. *Bull. Amer. Meteor. Soc.,* **95,** 1185–1199, doi:10.1175/BAMS-D-12-00225.1.

National Academy of Sciences, 2010: *Assessment of Intraseasonal to Interannual Climate Prediction and Predictability.* National Research Council, 192 pp.

Neelin, J. D., I. M. Held, and K. H. Cook, 1987: Evaporation–wind feedback and low-frequency variability in the tropical atmosphere. *J. Atmos. Sci.,* **44,** 2341–2348, doi:10.1175/1520-0469(1987)044<2341:EWFALF>2.0.CO;2.

Nordeng, T. E., 1994: Extended versions of the convective parameterization scheme at ECMWF and their impact on the mean and transient activity of the model in the tropics. Tech. Memo. 206, European Centre for Medium-Range Weather Forecasts, Reading, United Kingdom, 76 pp.

Palmer, T. N., F. J. Doblas-Reyes, A. Weisheimer, and M. J. Rodwell, 2008: Toward seamless prediction: Calibration of climate change projections using seasonal forecasts. *Bull. Amer. Meteor. Soc.,* **89,** 459–470, doi:10.1175/BAMS-89-4-459.

Pegion, K., and B. P. Kirtman, 2008: The impact of air–sea interactions on the simulation of tropical intraseasonal variability. *J. Climate,* **21,** 6616–6635, doi:10.1175/2008JCLI2180.1.

Rashid, H. A., H. H. Hendon, M. C. Wheeler, and O. Alves, 2011: Prediction of the Madden–Julian oscillation with the POAMA dynamical prediction system. *Climate Dyn.,* **36,** 649–661, doi:10.1007/s00382-010-0754-x.

Richards, K. J., M. E. Inall, and N. C. Wells, 1995: The diurnal mixed layer and upper ocean heat budget in the western equatorial Pacific. *J. Geophys. Res.,* **100,** 6865–6879, doi:10.1029/94JC03228.

Roeckner, E., and Coauthors, 1996: The atmospheric general circulation model ECHAM-4: Model description and simulation of present-day climate. Max-Planck-Institute for Meteorology Rep. 218, 90 pp.

Roundy, P. E., 2012: Observed structure of convectively coupled waves as a function of equivalent depth: Kelvin waves and the Madden–Julian oscillation. *J. Atmos. Sci.,* **69,** 2097–2106, doi:10.1175/JAS-D-12-03.1.

Roxy, M., 2014: Sensitivity of precipitation to sea surface temperature over the tropical summer monsoon region—and its quantification. *Climate Dyn.,* **43,** 1159–1169, doi:10.1007/s00382-013-1881-y.

Rui, H. L., and B. Wang, 1990: Development characteristics and dynamical structure of tropical intraseasonal convection anomalies. *J. Atmos. Sci.,* **47,** 357–379, doi:10.1175/1520-0469(1990)047<0357:DCADSO>2.0.CO;2.

Saha, S., and Coauthors, 2010: The NCEP Climate Forecast System Reanalysis. *Bull. Amer. Meteor. Soc.,* **91,** 1015–1057, doi:10.1175/2010BAMS3001.1.

Satoh, M., H. Tomita, H. Miura, S. Iga, and T. Nasuno, 2005: Development of a global cloud resolving model—A multi-scale structure of tropical convections. *J. Earth Simul.,* **3,** 11–19.

Seo, K. H., W. Q. Wang, J. Gottschalk, Q. Zhang, J. K. E. Schemm, W. R. Higgins, and A. Kumar, 2009: Evaluation of MJO forecast skill from several statistical and dynamical forecast models. *J. Climate,* **22,** 2372–2388, doi:10.1175/2008JCLI2421.1.

Shinoda, T., H. Hendon, and J. Glick, 1998: Intraseasonal variability of surface fluxes and sea surface temperature in the tropical western Pacific and Indian Oceans. *J. Climate,* **11,** 1685–1702, doi:10.1175/1520-0442(1998)011<1685:IVOSFA>2.0.CO;2.

Shukla, J., R. Hagedorn, B. Hoskins, J. Kinter, J. Marotzke, M. Miller, T. N. Palmer, and J. Slingo, 2009: Strategies—Revolution in climate prediction: A declaration at the world modeling summit for climate prediction. *Bull. Amer. Meteor. Soc.,* **90,** 175–178, doi:10.1175/2008BAMS2759.1.

Sobel, A., and E. Maloney, 2013: Moisture modes and the eastward propagation of the MJO. *J. Atmos. Sci.,* **70,** 187–192, doi:10.1175/JAS-D-12-0189.1.

——, ——, G. Bellon, and D. M. Frierson, 2010: Surface fluxes and tropical intraseasonal variability: A reassessment. *J. Adv. Model. Earth Syst.,* **2** (2), doi:10.3894/JAMES.2010.2.2.

Stephens, G. L., P. J. Webster, R. H. Johnson, R. Engelen, and T. S. L'Ecuyer, 2004: Observational evidence for the mutual regulation

of the tropical hydrological cycle and the tropical sea surface temperatures. *J. Climate,* **17,** 2213–2224, doi:10.1175/1520-0442(2004)017<2213:OEFTMR>2.0.CO;2.

Straub, K. H., 2013: MJO initiation in the real-time multivariate MJO index. *J. Climate,* **26,** 1130–1151, doi:10.1175/JCLI-D-12-00074.1.

Tao, L., X. H. Fu, and W. S. Lu, 2009: Moisture structure of the quasi-biweekly mode revealed by AIRS in western Pacific. *Adv. Atmos. Sci.,* **26,** 513–522, doi:10.1007/s00376-009-0513-2.

Tiedtke, M., 1989: A comprehensive mass flux scheme for cumulus parameterization in large-scale models. *Mon. Wea. Rev.,* **117,** 1779–1800, doi:10.1175/1520-0493(1989)117<1779:ACMFSF>2.0.CO;2.

Vitart, F., and F. Molteni, 2010: Simulation of the Madden-Julian Oscillation and its teleconnections in the ECMWF forecast system. *Quart. J. Roy. Meteor. Soc.,* **136,** 842–855, doi:10.1002/qj.623.

——, S. Woolnough, M. A. Balmaseda, and A. M. Tompkins, 2007: Monthly forecast of the Madden–Julian oscillation using a coupled GCM. *Mon. Wea. Rev.,* **135,** 2700–2715, doi:10.1175/MWR3415.1.

Waliser, D. E., 2005: Predictability of tropical intraseasonal variability. *The Predictability of Weather and Climate,* T. Palmer and R. Hagedorn, Eds., Cambridge University Press, 702 pp.

——, K.-M. Lau, and J.-H. Kim, 1999: The influence of coupled sea surface temperature on the Madden–Julian Oscillation: A model perturbation experiment. *J. Atmos. Sci.,* **56,** 333–358, doi:10.1175/1520-0469(1999)056<0333:TIOCSS>2.0.CO;2.

——, W. Stern, S. Schubert, and K. M. Lau, 2003: Dynamic predictability of intraseasonal variability associated with the Asian summer monsoon. *Quart. J. Roy. Meteor. Soc.,* **129,** 2897–2925, doi:10.1256/qj.02.51.

Wang, B., 1988a: Dynamics of tropical low-frequency waves: An analysis of the moist Kelvin waves. *J. Atmos. Sci.,* **45,** 2051–2065, doi:10.1175/1520-0469(1988)045<2051:DOTLFW>2.0.CO;2.

——, 1988b: Comments on "An air–sea interaction model of intraseasonal oscillation in the tropics." *J. Atmos. Sci.,* **45,** 3521–3525, doi:10.1175/1520-0469(1988)045<3521:COAIMO>2.0.CO;2.

——, 2011: MJO theories. *Intraseasonal Variability of the Atmosphere-Ocean Climate System,* 2nd ed. K. M. Lau and D. E. Waliser, Eds., Springer, 307–360.

——, and H. Rui, 1990a: Synoptic climatology of transient tropical intraseasonal convective anomalies: 1975–1985. *Meteor. Atmos. Phys.,* **44,** 43–61, doi:10.1007/BF01026810.

——, and ——, 1990b: Dynamics of coupled moist Kelvin–Rossby waves on an equatorial beta-plane. *J. Atmos. Sci.,* **47,** 397–413, doi:10.1175/1520-0469(1990)047<0397:DOTCMK>2.0.CO;2.

——, and T. Li, 1994: Convective interactions with boundary-layer dynamics in the development of a tropical intraseasonal system. *J. Atmos. Sci.,* **51,** 1386–1400, doi:10.1175/1520-0469(1994)051<1386:CIWBLD>2.0.CO;2.

——, and X. Xie, 1998: Coupled modes of the warm pool climate system. Part I: The role of air–sea interaction in maintaining Madden–Julian Oscillation. *J. Climate,* **11,** 2116–2135, doi:10.1175/1520-0442-11.8.2116.

——, T. Li, and P. Chang, 1995: An intermediate model of the tropical Pacific Ocean. *J. Phys. Oceanogr.,* **25,** 1599–1616, doi:10.1175/1520-0485(1995)025<1599:AIMOTT>2.0.CO;2.

Wang, J. D., W. Q. Wang, X. Fu, and K.-H. Seo, 2012: Tropical intraseasonal rainfall variability in the CFSR. *Climate Dyn.*, **38,** 2191–2207, doi:0.1007/s00382-011-1087-0.

Wang, W. Q., and K.-H. Seo, 2009: The Madden-Julian Oscillation in NCEP coupled model simulation. *Terr. Atmos. Oceanic Sci.,* **20,** 713–725, doi:10.3319/TAO.2008.09.17.01(A).

Watterson, I. G., 2002: The sensitivity of subannual and intraseasonal tropical variability to model ocean mixed layer depth. *J. Geophys. Res.,* **107,** 4020, doi:10.1029/2001JD000671.

Weaver, S. J., W. Q. Wang, M. Y. Chen, and A. Kumar, 2011: Representation of MJO variability in the NCEP Climate Forecast System. *J. Climate,* **24,** 4676–4694, doi:10.1175/2011JCLI4188.1.

Webster, P. J., and R. Lukas, 1992: TOGA COARE: Coupled Ocean–Atmosphere Response Experiment. *Bull. Amer. Meteor. Soc.,* **73,** 1377–1416, doi:10.1175/1520-0477(1992)073<1377:TCTCOR>2.0.CO;2.

Weller, R. A., and S. P. Anderson, 1996: Surface meteorology and air–sea fluxes in the western equatorial Pacific warm pool during the TOGA Coupled Ocean–Atmosphere Response Experiment. *J. Climate,* **9,** 1959–1990, doi:10.1175/1520-0442(1996)009<1959:SMAASF>2.0.CO;2.

Wheeler, M., and G. N. Kiladis, 1999: Convectively coupled equatorial waves: Analysis of clouds and temperature in the wavenumber–frequency domain. *J. Atmos. Sci.,* **56,** 374–399, doi:10.1175/1520-0469(1999)056<0374:CCEWAO>2.0.CO;2.

——, and H. H. Hendon, 2004: An all-season real-time multivariate MJO index: Development of an index for monitoring and prediction. *Mon. Wea. Rev.,* **132,** 1917–1932, doi:10.1175/1520-0493(2004)132<1917:AARMMI>2.0.CO;2.

Williams, K. D., and Coauthors, 2013: The transpose-AMIP II experiment and its application to the understanding of Southern Ocean cloud biases in climate models. *J. Climate,* **26,** 3258–3274, doi:10.1175/JCLI-D-12-00429.1.

Woolnough, S. J., J. M. Slingo, and B. J. Hoskins, 2000: The relationship between convection and sea surface temperature on intraseasonal timescales. *J. Climate,* **13,** 2086–2104, doi:10.1175/1520-0442(2000)013<2086:TRBCAS>2.0.CO;2.

——, F. Vitart, and M. A. Balmaseda, 2007: The role of the ocean in the Madden-Julian Oscillation: Implications for MJO prediction. *Quart. J. Roy. Meteor. Soc.,* **133,** 117–128, doi:10.1002/qj.4.

Wu, R., B. P. Kirtman, and K. Pegion, 2008: Local rainfall–SST relationship on subseasonal time scales in satellite observations and CFS. *Geophys. Res. Lett.,* **35,** L22706, doi:10.1029/2008GL035883.

Wu, Z. H., 2003: A shallow CISK, deep equilibrium mechanism for the interaction between large-scale convection and large-scale circulations in the tropics. *J. Atmos. Sci.,* **60,** 377–392, doi:10.1175/1520-0469(2003)060<0377:ASCDEM>2.0.CO;2.

Yanai, M., B. Chen, and W.-W. Tung, 2000: The Madden–Julian Oscillation observed during the TOGA COARE IOP: Global view. *J. Atmos. Sci.,* **57,** 2374–2396, doi:10.1175/1520-0469(2000)057<2374:TMJOOD>2.0.CO;2.

Yoneyama, K., C. D. Zhang, and C. N. Long, 2013: Tracking the pulse of the Madden–Julian oscillation. *Bull. Amer. Meteor. Soc.,* **94,** 1871–1891, doi:10.1175/BAMS-D-12-00157.1.

Zhang, C. D., 2005: Madden-Julian Oscillation. *Rev. Geophys.,* **43,** RG2003, doi:10.1029/2004RG000158.

——, 2013: Madden–Julian oscillation: Bridging weather and climate. *Bull. Amer. Meteor. Soc.,* **94,** 1849–1870, doi:10.1175/BAMS-D-12-00026.1.

——, M. Dong, S. Gualdi, H. H. Hendon, E. D. Maloney, A. Marshall, K. R. Sperber, and W. Q. Wang, 2006: Simulations of the Madden-Julian oscillation in four pairs of coupled and uncoupled global models. *Climate Dyn.,* **27,** 573–592, doi:10.1007/s00382-006-0148-2.

——, J. Gottschalck, E. D. Maloney, M. W. Moncrieff, F. Vitart, D. E. Waliser, B. Wang, and M. C. Wheeler, 2013: Cracking the MJO nut. *Geophys. Res. Lett.,* **40,** 1223–1230, doi:10.1002/grl.50244.